HHS Public Access

Author manuscript

Prog Neurobiol. Author manuscript; available in PMC 2022 August 21.

Published in final edited form as:

Prog Neurobiol. 2022 May ; 212: 102251. doi:10.1016/j.pneurobio.2022.102251.

Perceptual hue, lightness, and chroma are represented in a multidimensional functional anatomical map in macaque V1

Ming Li[1,2,3,*], **Niansheng Ju**[1,2], **Rundong Jiang**[1,2], **Fang Liu**[1,2], **Hongfei Jiang**[1,2], **Stephen Macknik**[4], **Susana Martinez-Conde**[4], **Shiming Tang**[1,2,*]

[1]Peking University School of Life Sciences and Peking-Tsinghua Center for Life Sciences, Beijing 100871, China

[2]IDG/McGovern Institute for Brain Research at Peking University, Beijing 100871, China

[3]State Key Laboratory of Cognitive Neuroscience and Learning, Beijing Normal University, 100875 Beijing, China

[4]State University of New York, Downstate Health Sciences University, 450 Clarkson Avenue, Brooklyn, New York, 11203 USA

Abstract

Humans perceive millions of colors along three dimensions of color space: hue, lightness, and chroma. A major gap in knowledge is where the brain represents these specific dimensions in cortex, and how they relate to each other. Previous studies have shown that brain areas V4 and the posterior inferotemporal cortex (PIT) are central to computing color dimensions. To determine the contribution of V1 to setting up these downstream processing mechanisms, we studied cortical color responses in macaques—who share color vision mechanisms with humans. We used two-photon calcium imaging at both meso- and micro-scales and found that hue and lightness are laid out in orthogonal directions on the cortical map, with chroma represented by the strength of neuronal responses, as previously shown in PIT. These findings suggest that the earliest cortical stages of vision determine the three primary dimensions of human color perception.

Keywords

Primary visual cortex; Color Perception; Functional map; Two-photon imaging; Macaque

1 Introduction

Trichromatic color vision in primates is advantageous to seeking food (Osorio and Vorobyev, 1996) and during social interactions (Chang et al., 2017; Freiwald, 2020a, 2020b; Hasantash et al., 2019; Hiramatsu et al., 2017; Shepherd and Freiwald, 2018; Sliwa and Freiwald, 2017). Different combinations of electromagnetic frequencies and intensities within the visible spectrum result in the colors we see, but colors are not seen as a linear function of wavelength and intensity. How the brain achieves the richness of color perception remains

*Corresponding author. mingli842@163.com(ML), tangshm@pku.edu.cn(ST).

a mystery. For more than one hundred years, artists and scientists have created various systems to describe the human perception of color. Most of them used dimensions of hue, lightness, and chroma, calling into question how human brains organize neural responses to produce these distinct dimensions of color perception.

The primary neural pathway of color signal processing is known (Conway, 2014; Shapley and Hawken, 2011). Three types of cone photoreceptors are differentially selective to overlapping bands of wavelength within the retina. Within the ascending retino-geniculo-cortical pathway, interactions between cone signals take place in both the retina (Dacey, 1996; Gouras, 1968) and in the lateral geniculate nucleus (LGN) (De Valois et al., 1966; Derrington et al., 1984). In V1, the subset of neurons that are selective to colors (Cottaris and De Valois, 1998; Lennie et al., 1990; Livingstone and Hubel, 1984, 1983; Thorell et al., 1984; Wachtler et al., 2003) concentrate within cytochrome oxidase (CO) blobs, in which cells preferring similar colors are often located in clusters (Garg et al., 2019; Landisman and Ts'o, 2002; Ts'o and Gilbert, 1988). In V2, hue-selective columns form band-like patterns in relation to the perceptual color wheel (Xiao et al., 2003). Downstream, V4 and the posterior inferotemporal cortex (PIT) are thought to fully represent perceptual color dimensions (Bohon et al., 2016; Conway and Tsao, 2009; Li et al., 2014). In the inferotemporal cortex (IT), cells with sharp tuning for saturation are also found (Komatsu et al., 1992), but whether chroma is represented by a pattern in a cortical map is unknown. The representation of perceptual color space appears to have developed gradually along the ventral visual pathway (Liu et al., 2020).

Subcortical opponent color processes undergo a nonlinear transformation in V1 (Cottaris and De Valois, 1998; De Valois et al., 2000; Horwitz and Hass, 2012; Stockman and Brainard, 2010), which instantiates the initial organizing principles of the primary three dimensions of perceptual color space processing in the brain. Anatomical evidence indicates that V1 layers II/III receive all three kinds of cone information (Sincich and Horton, 2005), and intrinsic signal optical imaging (ISOI) has shown that different hues activate organized cortical representations in V1 (Xiao et al., 2007). This suggests that neural populations in this area process different colors with segregated circuits. V1 moreover encodes hue and lightness in parallel (Hass and Horwitz, 2013; Johnson et al., 2001; Lennie et al., 1990; Livingstone and Hubel, 1988; Peng and Van Essen, 2005; Yoshioka et al., 1996) meaning that there could be a map of how different hue and lightness combinations are processed, with some V1 cells responses varying as a function of increased saturation (Hanazawa et al., 2000). In sum, previous studies indicate that V1 may contribute to the representation of all three perceptual dimensions of color. We thus initiated this project to determine V1's precise contribution to the organizing principles underlying color perception.

Various color systems have been used to study V1 responses, but near-uniform perceptual color spaces are rarely employed. Color gratings are often displayed to activate cells, especially as there has been great interest in understanding the relationship between orientation and color. In addition, most physiological studies of V1 have focused on equiluminant hue responses. Some studies have constrained lightness levels without controlling chroma, which could reduce response efficacy as a function of hue (Bohon et al., 2016). Notably, such methods are seldom used in human vision studies. Thus, to establish

a suitable correspondence between V1 responses in macaques and perceptual responses in human participants, we adopted a Munsell color space approach (Munsell, 1919), which is often employed in human color experiments.

Munsell color space consists of a central axis representing achromatic lightnesses between N_0 to N_{10}, with hue represented in the plane orthogonal to the lightness axis, and color chroma indicated with increasing distance from the central axis. Thus Munsell color space is geometrically cylindrical and it has the advantage of clearly defining and standardizing discrete points that can be used for human color perceptual testing. The orthogonal relationship between its color dimensions has moreover been verified as ecologically valid to human perception via multidimensional scaling (Indow and Kanazawa, 1960). Thus our use of Munsell color space allowed us to constrain the stimulus set of the current study to a defined and feasible range that nevertheless spanned the majority of human perceptual color space across all three dimensions. Although Munsell color space is not perfectly uniform perceptually, neither is any other color space. We overcame this drawback by also projecting color stimuli into various frequently used color spaces (such as CIELuv, CIE CAM2000). To further limit experimental complexity, we studied color space in isolation and did not examine its relationship to spatial response dynamics. Further studies will examine the important relationship between the color maps we have discovered and orientation maps.

Given the potentially small size of V1 color circuits, traditional techniques such as ISOI may not be precise enough to image the V1 representation of color space. Moreover, because many V1 cells are only partially tuned to color stimuli (Friedman et al., 2003), the low SNR of ISOI may prevent the reliable detection of all color-related responses. Though electrophysiological recordings may resolve some of these issues, they are themselves limited in that they do not provide the local sampling density or the spatial coverage necessary to map a large area of the cortex. Thorough mapping of multiple perceptual dimensions with electrophysiological approaches would also be time-consuming as it would require displaying an exceedingly large number of visual stimuli during the experiments. To overcome these difficulties, we used long-term two-photon imaging experiments in V1 (Li et al., 2017a) of two awake rhesus macaques (Macaque mulatta) in conjunction with the ultrasensitive genetically encoded calcium indicator GCaMP6s (Chen et al., 2013). We systematically mapped color perception in meso and micro scales in a restricted color space, by presenting carefully chosen color stimuli selected along with the hue, lightness, and chroma dimensions of Munsell color space (Munsell, 1919). Our data revealed that these dimensions are precisely represented in V1, and that there is a link between two-dimensional cortical color representation and three-dimensional perceptual color space.

2 Materials and methods

2.01 Experimental Design

Rhesus monkeys (Macaca mulatta) were purchased from Beijing Prima Biotech and housed at Peking University Laboratory Animal Center. The study used three healthy adult male monkeys, 4 – 5 years of age and weighing 5 – 7 kg. All experimental protocols were approved by the Peking University Animal Care and Use Committee.

The detailed procedures were described previously (Li et al., 2017a). Briefly, the animals were anesthetized, and a craniotomy was performed over V1 under sterile surgical conditions. The dura was reflected, and AAV vectors (AAV1.hSynap.GCaMP6s.WPRE.SV40, Penn Vector Core) were injected at multiple sites of the cortex, about 150 nL at each site. Injection sites were spaced at intervals of about 800 μm across the cortical surface. To avoid possible damage to the functional column structure, the injection pipette was inserted at an angle of 45 degrees to the surface. Within our 10 mm diameter imaging window, we completed 10 to 22 injections. The dura was then sutured, the bone flap replaced, and the skin was sutured. After 1–2 months, the animal was anesthetized again, the bone flap was removed under sterile conditions, and a durotomy was performed. A 2 cm-diameter round glass cover slip with a 1 cm-diameter titanium ring was positioned under the ~1 cm wide dura hole, with the titanium ring attached to the skull using dental cement, carefully applied to create a sealed imaging chamber that held the cover slip against the cortex. A large stainless-steel ring was attached with glue to the skull around the outside circumference of the craniotomy's edge (which allowed us to attach a cap to protect the chamber between recordings). A custom three-point head stabilization halo was implemented to minimize motion of the skull during recordings. We mounted three head posts at roughly equidistant points around the circumference of the skull: two on the left and right temples respectively, and one on the back of the skull. These three points formed a plane, and during recordings, were connected to a heavy steel plate with T-shaped braces positioned under the microscope as part of the monkey chair assembly. Following the implantation surgery, the animals recovered in the vivarium for one or more months.

During imaging procedures, each monkey was seated in a primate chair under the microscope. Each monkey fixated on a small white spot (0.1°) within a window of 1° for over 2 s to obtain a juice reward. Eye positions were monitored with an infrared eye-tracking system (ISCAN) at 120 Hz.

Visual stimuli were generated using a ViSaGe system (Cambridge Research Systems, UK) and displayed on a 21-inch CRT monitor (SONY G520, refresh rate = 80 Hz, maximum luminance = 105 cd/m^2). The CRT was positioned 51 cm away from the eyes of the animals and calibrated for precise color emission as described below. The V1 neuronal receptive field (RF) sizes and positions (ranging from 2.7° to 4.8° of eccentricity within the monkeys' visual fields) were estimated using manual mapping with black and white dots.

2.02 Visual Stimuli

We employed a set of 93 different visual stimuli to determine the stimulus preference of each cell (Fig 1E). Orientation and color preference was determined with drifting Gabors (SF = 3 cycles/degree, speed = 2.67 cycles/second, σ = 0.25°, and contrast = 100%) or static color disks (1° in diameter), respectively. Each Gabor or disk stimulus was presented for one second following a one-second blank interval, once fixation was voluntarily initiated by the monkey. All stimuli were shown against a background of either homogenous gray (Munsell color N_5) or a mosaic of randomly chosen achromatic dots with Munsell colors N_0 to N_{10}. Randomly chosen backgrounds were re-randomized for each presentation and balanced to

equal an average luminance of N_5. Ocular dominance (OD) was determined by alternately presenting achromatic gratings to each individual eye.

2.03 Calibration of CRT chromaticity in CIE coordinates

We used an automated closed-loop system to establish the proper RGB values for a given CIE coordinate's chromaticity with our video stimulation system's CRT. Each specified stimulation color from our set of 93 stimuli was assigned target coordinates for the calibration function (x_t y_t Y_t). We then presented a one-degree patch of the stimulus on the CRT with an initial arbitrary RGB test value and measured the video output with a SpectroCAL spectroradiometer (Cambridge Research Systems, UK). We corrected the error between the measured and desired CIExyY coordinates by adjusting the RGB values to reduce the error function (***e***), followed by a retest, using this formula:

$$e = \sqrt{\left(\frac{x_c - x_t}{x_t}\right)^2 + \left(\frac{y_c - y_t}{y_t}\right)^2 + \left(\frac{Y_c - Y_t}{Y_t}\right)^2}$$

Let x_c, y_c, and Y_c be the measured CIExyY coordinates. This search algorithm repeated until the error was optimized to a level below 1% (e > 0.01), within the CRT's RGB color space of ($R \pm 1,\ G \pm 1,\ B \pm 1$). Once $e \leq 0.01$ for each color and achromatic stimulus in our set, the RGB values were stored for use in our experiment.

2.04 Munsell color space parameters

To calibrate our chromatic stimuli to specific points within Munsell color space, we obtained the CIE_1931 xyY coordinates for each Munsell color from the Munsell Color Science Laboratory of Rochester Institute of Technology (RIT, https://www.rit.edu/cos/colorscience/rc_munsell_renotation.php). To test the lightness response of various hues while holding chroma stable, we chose Chroma level 6. This was based on our preliminary data showing that peak SNR in neuronal calcium signal responses occurred when chroma levels were significantly below ceiling (Fig. 3F). This choice allowed us to achieve the most linear possible neural responses as a function of lightness across the entire stimulus set without saturating.

We note that Chroma 6 of some stimuli could not be produced by our CRT (due to its limited gamut), for a subset of lightness levels. This typically occurred at the extremes of the Munsell Value range (i.e., one and/or nine, see Fig. 1A). To estimate Chroma at the extreme ranges of our CRT, we fit splines to both the x and y coordinates listed within the RIT Munsell Color table and interpolated the intermediate chroma levels from the coordinate curves at a resolution of 0.1. We then employed the maximum chroma level achievable using our closed-loop color calibration system (above) during the experiments (see Tables 1 and 2).

2.05 Calculation of stimulus color coordinates and DeltaE in other color spaces

To calculate DKL coordinates for our color stimuli, we measured the spectrum of our CRT (S_{CRT}) using the same spectroradiometer used to calibrate the CRT's chromaticity.

Color matching functions (CMFs) (Stockman & Sharpe cone fundamentals 2000, 10 degrees) (Stockman and Sharpe, 2000) were obtained from Color and Vision Research Labs (http://www.cvrl.org). The transformation from RGB to LMS was defined as LMS = CMFs' * S_{CRT} * RGB'. These LMS coordinates were transformed into DKL coordinates by *lms2dkl* function in the toolbox of "Computational Color Science using MATLAB" (Peng and Van Essen, 2005). We converted each stimulus's CIExyY coordinates into CIEXYZ coordinates, and to other color spaces, using the "Computational Color Science using Matlab" toolbox. In DKL and Munsell color spaces we defined DeltaE as the Euclidean distance between colors. When using other color spaces, we defined DeltaE following their specific conventions.

2.06 Two-photon imaging

Two-photon imaging was performed using a Prairie Ultima IV (In Vivo) microscope (Bruker Nano, GmbH, formerly Prairie Technologies) driven by a Ti: Sapphire laser (Mai Tai eHP, Newport Spectra-Physics Ltd). The wavelength of the laser was set to 1000 nm. The objective lens was either 16X (N.A. = 0.8, Nikon), 25X (N.A. = 1.05) or 4X (N.A. = 0.2, Nikon). Laser scanning employed a combination of galvanometers (galvos) and resonance frequency scanners (resonant) to sweep the laser across x and y positions within each z-axis depth to create an image at each depth. To obtain static images with high resolution (1024 × 1024), we used galvos for both x and y positioning, which resulted in slow scans (~1 sec / frame). We used fast resonant-galvo scanners (up to 31.5 frames per second) to obtain calcium response time-series (resolution 512 × 512) of neuronal activities (typically, 8 fps while employing online averaging of every four scanned frames). We did not observe any cortical damage in long-term recordings using the 4X objective with 90 mW laser power on the cortex.

Due to the difference in signal-to-noise (SNR) for each of the three different objectives, the number of trials used to sample functional responses varied by objective type (N = 10–11 for 16x or 25x objective data, N = 50 for 4x data).

2.07 Overall image analysis paradigm

To establish the functional anatomy of color processing in V1 from microscopic data acquired at varying resolutions, we analyzed the data at multiple spatial and temporal scales, as described in the following sections. In summary, we first pre-processed the raw image files to determine the image pixels that we later analyzed for functional activity. We grouped those pixels in three ways. First, we determined meaningful cellular shapes for the identification and screening of individual cells (cellular maps)—this allowed us to analyze individual cell response time courses for some of the analyses. Second, to create functional anatomical maps of stimulus selectivity we binned raw pixels 2 × 2 and determined fluorescence responsivity to visual stimuli (i.e., $\Delta F/F$ maps). We used these pixel-by-pixel response time-series to analyze both raw calcium responses and to create functional maps of perceptual selectivity such as hue and orientation. Third, we established the statistical significance of newly discovered functional maps relevant to color perception (such as hue and lightness) by analyzing clusters of significantly responsive pixels. We conducted several further statistical analyses to better understand the data in a variety of

ways, such as classical multidimensional analysis and other tests of statistical significance of the results, as described below.

2.08 Image data pre-processing

We analyzed data using customized MATLAB code (The MathWorks, Natick, MA). We continuously recorded from an imaging plane during a calcium recording session, producing a time series (TS) of images that could be related to the synchronized stimulus presentation. To address motion artifacts during long recordings, we analyzed the first 5000 images of each TS and averaged the 10% most correlated images to create a template image. The remaining images were then motion-corrected using this template by normalizing with a cross-correlation-based translation algorithm (Li et al., 2017b). Eight averaged frames (about 1 second in recording duration) before and after each stimulus onset were averaged to form the F0 and F1 frames of a stimulus response, respectively. Cellular and response extraction for all subsequent analyses followed from a primary initial procedure: we spatially binned pixels 2 × 2 to enhance SNR by reducing noise (examples in Fig. 1H and I).

2.09 Signal to noise ratio

Signal to noise ratio was defined by $\mathrm{SNR} = \frac{\mu_{max} - \mu_{min}}{SE_{max} + SE_{min}}$, where μ_{max} and μ_{min} were the mean responses to the best and worst stimuli. SE_{max} and SE_{min} were the corresponding standard errors (Nauhaus et al., 2012). SNR was computed pixel-by-pixel to get a raw SNR map. This raw SNR map was smoothed (Gaussian filters, $\sigma = 35$ μm) to cover or exclude regions with SNR < 3 (Fig. 5B and C). This was applied to calculate the functional maps described in the "Functional mapping analyses" section below.

2.10 Functional mapping analyses

We conducted three different types of basic pixel-by-pixel analyses to study the responsivity of our TS to our 93 individual stimuli. First, we calculated the pixel-by-pixel SNR of these responses (see above). Second, we calculated the average calcium responses over multiple trials and used them to produce $\Delta F/F$ maps (examples in Fig. 1F and 1G), where $\Delta F/F = \frac{\sum_{fi=1}^{n} (F1_{fi} - F0_{fi})}{\sum_{fi=1}^{n} F0_{fi}}$ and n ($n \geq 1$) was the number of stimulus conditions. Finally, the statistical significance of the map was determined with a Student's t-test comparing the F1 and F0 means for each pixel's response to each stimulus (described in more detail in the "Identification of clustered patterns with connected component labelling" section below). The average ΔF/F maps for orientations versus hues were computed and normalized. Peaks on these maps were thresholded (0.75), and pixels within the union of the peak regions were compared by Pearson correlation (Fig. S1E).

2.11 Cell extraction and screening

A temporal response analysis was created for each cell (rather than for each pixel in each image), by identifying the individual cells in each image and deriving a time-course of their responses as a function of visual stimulation. Responsive cells for each stimulus condition

were identified as round regions of interest (ROIs) that exhibited calcium responses, using the $\Delta F/F$ maps described above. We set the radius (r) of each ROI manually (r = 5.5 μm; for 16x, r = 3.5 pixels; for 25x, r = 5.5 pixels). We convolved the $\Delta F/F$ maps with a difference-of-gaussians (DOG) filter ($\sigma 1$ = 0.25 * r, $\sigma 2$ = r) and binarized the results using the triangle threshold method (Zack et al., 1977). We defined the ROIs from these binary maps as responsive cells. ROIs which were too large ($area > \pi * (2r)^2$) or too small ($area < \pi * (r/2)^2$) or not round (with round index $4 * \pi *$ area / perimeter$^2 < 0.5$) were discarded. We applied a mask defined by these ROIs to the raw image frames to obtain the fluorescence responses to each stimulus and determined the aggregate average ROI response by averaging the ROI's pixels. The ratio of fluorescence changes (cellular $\Delta F/F$) was thus defined as the response to a stimulus. We identified visually responsive cells by discarding cells that did not exhibit significant response selectivity for any of the 93 visual stimuli that we presented (tested with a one-way ANOVA, $p > 0.01$). We subsequently identified color-responsive cells (hue, lightness, and chroma responsivity) using the same ANOVA test, by restricting the test to the responses from the specific chromatic stimuli.

2.12 Pixel map creation

We created various pixel-based maps (rather than cell-based maps) of functional preference from the 2 × 2 binned $\Delta F/F$ maps, in which every pixel in the image was assigned a preference. These maps were created by examining the functional responses to different subsets of our 93 stimuli set (hue, lightness, orientation, and chroma), to produce 4 different functional preference maps. Note that chroma did not produce a spatial map and was revealed to be represented by the magnitude of the functional response (see analysis below). To create pixel maps from the $\Delta F/F$ maps, we determined the response of each pixel to the appropriate stimuli for each functional type. The stimulus which activated a given pixel most powerfully was assigned as the pixel's preferred stimulus for each functional map's stimulus dimensions. That is, each individual pixel, within each of the four different pixel maps, was assigned a preference for hue, orientation, lightness, and chroma. These pixel maps were later used as the basis of statistical analyses to extract the presence of pinwheels, linear zones of response, etc. (see below).

After we obtained the pixel maps of hue or orientation (Figs. 2A, 2B, S2A and S2B) we computed the gradient of hue or orientation angles at each pixel. To address potential gradient discontinuities at the edges of the angle maps (for example, when π meet – π), we created a copy of the angle map and converted the values between [-π 0] to [π 3π] and recomputed the gradients near the discontinuous edges. Within pinwheels the gradients are similar to the velocity fields of a vortex. Following from Graftieaux (2001), we computed the vortex index of each pixel of the angle gradient map using an ROI of 19×19 pixels: For each pixel within an ROI, a radial vector map was created by using vectors from the center of the ROI to each pixel. At each pixel position, we then computed the sine of the angle between the gradient and the radial vectors. The mean value of the sine values within an ROI constituted its vortex index. The absolute value of the vortex index of each pixel on the angle map formed a vortex index map. Within pinwheel positions we found the vortex index to be quite close to 1. A threshold of mean + 5*SD was used to isolate the pinwheel positions.

2.13 Identification of clustered patterns with connected component labelling

We identified significant pixels by comparing the *F0* and *F1* responses from 2 × 2 binned pixels with one-tailed Student's t-test ($p < 0.01$, though sometimes when the significant pixels were densely packed, we employed a significance threshold of $p < 0.001$ or 0.0001).

We grouped visually responsive pixels into clusters using the OPTICS algorithm (Python package scikit-learn 0.24.2). We generally employed the default parameters in OPTICS, except for *min_samples* and *min_cluster_size*. These parameters were estimated in the following way. First, contiguous pixels within the significant pixel map were identified as objects using the MATLAB *bwconncomp* function. Identified objects were then sorted in descending order by the number of pixels in each object. The threshold was then identified by determining the "elbow" in the size frequency distribution, using a triangle threshold algorithm (Zack et al., 1977). This "elbow" in the frequency distribution was assigned as the OPTICS variable*: min_samples*, and thus smaller objects were filtered out. We defined the OPTICS clustering variable *min_cluster_size* empirically as *min_cluster_size* = 10 x *min_samples* +100.

We assigned convex hulls to each of the clusters to identify them as visually responsive regions of cortical activity for subsequent analyses of chromatic and orientation tuning (examples in Fig. 1H). The centroid (center-of-gravity) of each contour was defined as the position of the average response-weighted pixel within each contour. We refer to these stimulus-tuned contours as patches for subsequent analysis.

2.14 Grouping of hue, lightness, chroma, or achromatic patches

To analyze the spatial relationships on the cortex between stimulus-tuned patches identified in the previous section, we grouped patches as a function of their density as defined by the OPTICS algorithm. We grouped using four dimensions: hue, lightness, chroma and achromaticity.

Because noise was rejected at the cluster level (see previous section), we did not have a noise-rejection stage, and thus *min_samples* was set to the minimum value (2); *min_cluster_size* was set to *round(Nstim * 80%)*. On the rare occasion that more than one patch centroid within a group had the same stimulus preference, we discarded the redundant patch (Figs. S2E and S3). We omitted redundant patches by identifying those that were far from the rest of the group.

2.15 Cortical distances between centroids of patches

The distance between similarly and differently tuned functional patches is a critical analysis in understanding the underlying circuits in cortex. To compute cortical distances between hues, lightnesses, and levels of chroma, we calculated the pairwise Euclidean distance between all centroids within each group. We then pooled these pairwise distances across groups to determine the median distances and variability (Figs. 2G, 3E, and 4F).

2.16 Classical multidimensional scaling (cMDS) of cortical distance

The pairwise patch distance information lends itself to similarity analyses using cMDS; we used the Matlab function *cmdscale*. We calculated cMDS coordinates between patches of a single stimulus dimension using the median distances between patches of that stimulus type. To assess the spatial structure of patches of two or more stimulus dimensions on the surface of V1, we compared the median distances between all pairwise patches from various combinations.

The stress factor in the cMDS analysis is computed as $stress = \sqrt{\frac{\sum\left(d_{ij} - \widehat{d_{ij}}\right)^2}{\sum d_{ij}^2}}$, where d_{ij} is the distance in the original matrix. $\widehat{d_{ij}}$ thus represents the distance in the MDS constructed space. We adopted the first two or three dimensions to compute the $\widehat{d_{ij}}$ in this analysis.

2.17 Multidimensional scaling (MDS) of stimulus dissimilarity in neuronal space

Because each visually responsive neuron could potentially have a complex response profile to the various color stimuli we presented, we considered each neuron as a dimension in our analysis, with the number of dimensions of the resultant multidimensional space being the number of neurons recorded. A given stimulus typically activated many neurons with different strengths, and the population response profile of each stimulus was assigned as a coordinate within this multidimensional neuronal space. To compute the similarity between each of our 81 color stimuli in a pairwise fashion, we calculated the correlation between responses from all the neurons for each stimulus pair. We obtained the MDS of color responses by first building an 81 × 81 similarity correlation matrix (*Ms*) using the coordinate responses to the subset of 81 color stimuli. Finally, the dissimilarity matrix was defined as *1–Ms* for the MDS calculation using the Matlab *mdscale* function, employing *'sammon'* criterion. The stress of MDS was obtained directly from the output of this *mdscale* function.

Shepard plots further visualized the goodness of the MDS within specific dimensions by indicating how well the distance in the MDS space reflected *1-Ms* (Fig. S6).

2.18 Hue-lightness contour maps and their orthogonality

We derived two separate pixel maps from the hue-lightness preference map (Figs. 5A and S5A), one for hue and one for lightness. These pixel maps were smoothed by gaussian low pass filters (sigma = 35 μm) and hue and lightness were then discretized into 5 and 11 levels respectively and plotted as contours (isoheight lines) onto a single map (Figs. 5C and S5C). Points of crossing between the hue and lightness contours established the degree of orthogonality between lightness and hue maps. We calculated the separate gradients along the hue and lightness dimensions at the crossing-points, and the difference in the direction of each crossing gradient was calculated and plotted as a histogram in Fig. 5D.

To evaluate the significance of the peaks on the histogram, we permutated the stimuli tags randomly and repeated the above analyses with 1000 iterations. The maximum value on the left versus right halves of the histograms were then used to test the significance level of the difference between peaks.

2.19 Multiple linear regression analysis of cellular color responses

To quantify whether V1 cells are described better by Munsell versus DKL color space, we fit cellular responses to color stimuli with multiple linear regressions derived by the coordinates of the color stimuli within each color space (Fig. 7A and Fig. S7). In Munsell color space, x and y coordinates of a stimulus was defined by x = Chroma * cos($Angle_{hue}$), y = Chroma * sin($Angle_{hue}$), z = Munsell Value, whereas in DKL color space, x = L - M, y = S - (L + M), z = L + M. We also fit a reduced multiple linear regression model using solely equiluminant colors (all the color stimuli with Munsell Value = 5), where only x and y coordinates were considered.

To determine any spatial differences between Munsell vs DKL preferring cells, we first identified cells that were more selective to Munsell color space than to DKL color space ($R^2_{Munsell} > R^2_{DKL}$ and $R^2_{Munsell} > 0.5$; left panels of Fig. 7B). We compared these to the general color-selective or orientation-selective local calcium response patches—LoCa patches (see Section 3.1 for details on how LoCa patches are determined). Munsell-encoding cells were largely confined to color selective LoCa patches of cortex. We then identified those cells that exhibited preference for DKL color space over Munsell space ($R^2_{DKL} > R^2_{Munsell}$ and $R^2_{DKL} > 0.5$; left panels of Fig. 7C) and compared them with color-selective or orientation-selective LoCa patches. DKL-encoding neurons were found largely within the regions where color- and orientation-selective LoCa patches overlap.

To quantify these findings, we converted the pixel values to z-scores for a large cortical area of LoCa maps representing color or orientation fields. Then z-score values at the positions of specific subpopulation of cells were collected and shown as histogram (Fig. 7D–E). At last, z-scores collected from the color field maps were compared with those collected from the orientation field maps, mean values of these z-scores collected from different maps were tested by Student’s t-test.

2.20 Statistical Analysis

We employed the Student’s t-test to determine significant responses in pixels by comparing fluorescent intensity before and after stimulus onset. We compared medians with a Wilcoxon rank-sum test. We quantified correlations using Pearson’s correlation, and compared the correlation coefficients using Williams’ t-test (Williams, 1959). We corrected multiple testing using Bonferroni correction.

3 Results

3.1 Visual stimuli and recording procedures

Due to the vast size of Munsell color space, and because we needed to run multiple trials of each stimulus to achieve sufficient SNR in our responses, we could not test every combination of hue, chroma, and lightness. Instead, we reduced the number of stimuli to cover all three dimensions (Fig. 1A) and we focused our studies on: 1) 11 achromatic lightness levels along the central axis of Munsell color space (N0 to N10); 2) five hues that are roughly evenly spaced around the color wheel of perception (Munsell 5R, 5Y, 5G, 5B, and 5P) as a function of four to seven chroma levels (in which lightness was held constant at

level 5); and 3) the same five Munsell hues as a function of nine lightness levels (in which chroma was held constant at level 6). The implementation of iso-chroma levels is an advance over previous color recordings in V1 (Garg et al., 2019; Xiao et al., 2007). In addition, we presented achromatic drifting gratings in six different orientations and two directions (Fig. 1B) to assess orientation selectivity. There were thus 12 oriented gratings + 11 achromatic Munsell stimuli + 25 Hue/Chroma Munsell stimuli + 45 Hue/Level Munsell stimuli = 93 stimuli in total.

Our imaging methods follow our previous studies (Ju et al., 2020, 2018; Li et al., 2017a; Liu et al., 2020). Fluorescence responses to stimuli were defined as *(F1-F0)/F0—ΔF/F—* where *F0* and *F1* were fluorescence signals averaged over a period of one second before versus after stimulus onset, respectively. The presentation of one stimulus constituted a trial, and each of 93 stimuli was presented 10–11 times at each cortical imaging location. We used a 16X or 25X objective lens, and after motion correction (Li et al., 2017a), the images were stable within a given recording session (Fig. S1). Over the course of the entire experiment, we recorded approximately 1000 successful trials for a single imaging plane on each cortical location. Individual cells varied in their preferences within different dimensions of our stimulus set (Fig. 1E). We identified color-tuned patches (Fig. 1F, averaging of 5 hues) by the *ΔF/F* Ca responses from cellular neuropil and somas—we refer to these maps as “local cortical calcium responses” (LoCa maps). The cortical surface area of the LoCa patches ranged from tens to hundreds of square millimeters. By comparing F1 with F0 pixel-by-pixel across 10–11 repeat trials for each stimulus (Fig. 1G, one-tailed paired-sample t-test, $p<0.01$), we identified significantly activated pixels and clustered them into patches using the OPTICS algorithm (Ankerst et al., 1999). We created convex hulls around these identified clusters to indicate specific LoCa patches, following the analyses described in the Materials and Methods. Different hue stimuli activated patches located at different positions of the cortex (Fig. 1H and 1I).

3.2 Pinwheels and linear zones of hue-selectivity in V1

Using a 4X objective lens (3.2 mm x 3.2 mm field of view), we recorded robust mesoscale calcium signals and obtained high-resolution ocular dominance (OD) maps (white lines in Fig. 2A). We obtained both color and orientation pixel maps (Figs. 2 and S2, see Materials and Methods) by mapping responses to either the five Munsell hues (Value = 5, Chroma = 6) or the orientated gratings. Although there was overlap, the peak color-selective regions were negatively correlated to the peak orientation-selective regions ($r \leq -0.55$ across both monkeys, Fig. S1E). This corroborates previous studies showing that color-sensitive cortical regions are segregated from orientation-selective regions in V1 (Garg et al., 2019; Livingstone and Hubel, 1988). We tended to find that hue-selective patches, rather than being isolated, were grouped with patches selective to many other hues. Groups of hue-selective patches formed either pinwheel-like patterns (for example, Fig. 2A site 1) or linear zones (for example, Fig. 2A site 2). Both in hue pinwheels and linear-zones, hues were typically arranged in spectral order, with patches selective to a given color generally abutting patches selective to cooler chromatic hues on one side and to warmer hues on the other. The centers of the pinwheels were identified with a vortex detection algorithm ((Graftieaux et al., 2001), see Materials and Methods). Just as peak hue-selectivity was anti-correlated with

peak orientation-selectivity, hue-pinwheel centers did not overlap with orientation-pinwheel centers (Figs. 2C and S2C).

Our analyses included three different mapping procedures, each of which with a different set of advantages. First, pixel maps are highly informative about patterns of activity across the surface of the cortex, but they have relatively low SNR and are potentially susceptible to image processing artifacts (i.e., pinwheels can be found in noise). Second, whereas cellular maps represent the ground truth of neuronal response selectivities in two-photon imaging, the number of cells in a imaging plane is sparse, making cellular maps relatively poor for the study of patterns of activity across large circuits. Third, LoCa maps (contour maps) have the advantage of identifying regions of similar activity across the cortical surface for large pattern analyses, but they are not informative as to the specific source of the signals. To ensure the validity of our pixel and contour maps, we compared them to the cellular responses from a volume having 7 imaging planes. We found that, irrespective of the analysis approach, hue maps did not differ (Fig. 2D–F). This verified that our novel pixel and contour mapping methods faithfully represent neuronal selectivities made with traditional cellular mapping techniques.

Pinwheel-like structures were consistent with perceptual color-wheels. We also noticed that patches at the terminals of the linear zones were not selective to random hues. Instead, the internal structure of the linear zones otherwise obeyed perceptual relationships. To test the overall relationship of these hue representation structures, we grouped the patches by OPTICS clustering (Fig. S2D and S2E) and analyzed the distance between patches of different hues (see Materials and Methods). For monkey A, the median distance was 69.39 ± 4.99 μm (n = 126, median ± 1.57 * IQR / sqrt(n)) between adjacent hues and 106.45 ± 7.82 μm (n = 124, median ± 1.57 * IQR / sqrt(n)) for non-adjacent hues. For monkey B, those distances were 41.31 ± 6.43 μm (n=130) and 79.62 ± 7.8 μm (n = 130), respectively. In both monkeys, the distances between non-adjacent hues were significantly larger than between adjacent hues (one-tailed Wilcoxon rank-sum test, $p < 0.05$).

We used classical multidimensional scaling (cMDS) to reconstruct the positions of 5 hues according to their distance (Fig 2H, see Materials and Methods). Stress at dimension 2 was 0.06 and 0.13 for monkeys A and B respectively, meaning that the distances between patches within the first two dimensions of cMDS were highly coincident with the physical cortical distances between patches. Because cMDS optimizes the geometry of a specified set of related distance vectors, this outcome suggests that V1 optimally represents the perceptual similarity of hues in its cortical map. Specifically, the reconstructions showed that the 5 hues tested were distributed in rough accordance to their perceptual relationship to each other. That is, whereas the outcome might have been any order combination of the 5 hues, we found that the relationship generally followed spectral order, which may explain why perceptual relationships follow spectral (physical) wavelength order. To quantify this relationship we computed the linear correlation coefficient between the median cortical distances of the 5 hues and their perceptual DeltaE in various color spaces (Fig. 2I). In both monkeys, the distances were highly correlated with the near-uniform perceptual color spaces we tested, including Munsell, CIELUV, CIELAB, and CIE2000. The correlation was also significant with CIExyY color space in monkey B, but not in monkey A, perhaps due to

the limited number of hues we used in our stimulus set, or because of the poor perceptual uniformity of CIExyY color space. The correlation was not significant for DKL color space, suggesting that whereas the retina may organize color along dimensions of cone sensitivities (central to the organization of DKL color space), V1 cortical circuits may not.

Together, our combined results indicate that primate hue perception is consistent with V1 hue representations as a function of cortical distance.

3.3 The map of Munsell lightness in V1

Lightness is a primary dimension in color space. The background lightness adaptation state significantly affects the neural response to various relative luminance levels (relative to lightness) (Peng and Van Essen, 2005). We investigated the effect of local versus average background contrast by using two different background configurations: a homogeneous gray field (Munsell color N5) versus a mosaic background composed of small achromatic squares (0.13° x 0.13°) having randomly varied lightness levels (Munsell colors N0 to N10), with an average lightness equivalent Munsell color N5. The background configuration had a significant effect on the distribution of achromatic patches on the cortical surface (Fig. 3 A–C). With the gray background, the stimuli that were lighter than the background produced cortical patches gathered into a bright grouping, whereas the stimuli that were darker than the background produced cortical patches gathered into a separate dark grouping (upper row of Fig. 3A and C, Fig. S3A). These groupings are reminiscent of the ON and OFF columns previously reported in cat and monkey V1 with electrophysiological (Kremkow et al., 2016) and two-photon imaging (Lee et al., 2016) methods. Under the mosaic background, achromatic lightness was represented by a systematic and graded displacement of cortical patches (lower row of Fig. 3A and C, Fig. S3B), forming linear zones of achromatic lightness. This suggests that local and average background contrasts have different effects on achromatic color processing.

Local versus average background contrast stimuli did not, however, have different effects on cortical representations of chromatic lightness. We moreover did not observe a pattern such as ON and OFF columns arise to represent chromatic lightness while using either homogenous or mosaic backgrounds (Fig. S3C). Instead, we found that patches representing different chromatic lightnesses formed linear zones irrespective of the background (Figs. 3D and S3D). These color lightness representations were consistent with the cellular and pixel maps we found through different analysis methods (Fig. 3E and S3E). To establish the relationship between these cortical locations quantitatively, we pooled together the cortical pairwise displacements found for each patch (see Materials and Methods). We found that as the lightness level decreased, the activated patches moved gradually from white patches to dark patches (Fig. 3F). For a specific group of lightness patches, the linear zones of lightness were rooted either between the achromatic white and black preferring regions of cortex or with at least one white/black region at one end of the chromatic lightness patch grouping.

To quantify the relationship of lightness-tuned regions of the cortex to perception, we computed the correlation coefficient between cortical distances of lightness patches and DeltaE in various color spaces (see Materials and Methods). The correlations with near-uniform perceptual color spaces, including Munsell, CIELUV CIELAB, and CAM2000,

were significantly larger than with DKL and CIExyY color spaces (Fig. 3G). This suggests that the representation of lightness across the surface of the cortex is mapped consistently with perception.

We also note that the lightness linear zones aligned well across pixel maps, LoCa maps, and cellular maps (Fig. 3E). This finding shows that the lightness results are robust to the mode of analysis (Fig. S3F).

Macroscopic chromatically-tuned lightness representations have not been reported previously, to the best of our knowledge. To establish reproducibility, we compared the pixel maps created from data acquired in different experimental sessions across many days. The maps remained stable even when the recordings were obtained weeks apart (Fig. S3G).

3.4 Chroma is represented by the strength of the neural response

We tested whether chroma levels were represented by tuned patches at different cortical locations. We analyzed responses to chroma stimuli while holding the background lightness stable (homogenous gray backgrounds in monkey A and mosaic backgrounds of the same average lightness in monkey B). However, we did not find a significant number of chroma-tuned cells or hue patches that systematically varied in cortical location as a function of chroma. Instead, the signal strength of the neuronal response increased as chroma level increased (Fig. 4A–C). Most cells moreover preferred the saturated chroma levels (Fig. 4B). Only 1.97% of the cells (19/966, two-tailed Student's t-test, $p < 0.05$) preferred submaximal chroma levels. Therefore, few cells were selective for unsaturated colors in layers II/III of V1, consistent with previous findings (Hanazawa et al., 2000).

We analyzed hue patches more extensively to determine if there was an internal cortical microstructure within patches that mapped chroma at a level not identified with our previous analyses. We found that varying chroma levels did not alter the center of gravity of hue patches and did not result in subclusters of chroma-tuned responses positioned at different cortical locations (Fig. 4D). The cortical locations of hue patches were stable across chroma levels larger than 6 (Fig. 4E). Any displacements found with low chroma levels were accounted for by decreased signal-to-noise, which inevitably reduced the size of contours, thus affecting the precision of the patch locations (Fig. 4C).

To determine the relationship between chroma signal strength and perception, we compared the LoCa response strength (Fig. 4F) to the distance (DeltaE) in various color spaces (see Materials and Methods) and found them to be positively correlated (Fig. 4G). In addition, signal strength was more highly correlated to DeltaE of human perception-based color spaces than to the antagonistic-mechanism-based DKL color space (Fig. 4G).

These analyses indicate that the perception of chroma is represented in V1 layers II/III by neural response magnitude rather than by cortical location.

3.5 Cortical Representations of Hue and Lightness are Orthogonal to Each Other

To investigate how hue and lightness maps interact spatially across V1's cortical surface, we generated mesoscale pixel maps of hue and lightness preference (Figs. 5A and S5A). After

applying a low-pass Gaussian filter (σ = 35 μm) and using iso-contours to view the data, the orthogonality of the hue versus lightness interactions were evident (Figs 5B–C and S5B–C). We quantified their spatial relationship as the angle difference at each hue/lightness contour crossing point on the map (see Materials and Methods). This procedure revealed clear peaks at about +/−90 degrees (Fig. 5D).

We also assessed the orthogonality of the hue and lightness maps using cMDS. We created the cMDS space using the lightness patches, including both chromatic and achromatic lightness patches (excluding achromatic N5) and removed noise by excluding outlying patches in the lightness dimension identified by the OPTICS algorithm (see Materials and Methods). We created a distance matrix by finding the distances between the centers of gravity of these patches (see Materials and Methods). We further analyzed the first three cMDS dimensions (stress = 0.03 in monkey A, 0.02 in monkey B at the third dimension) to determine the orthogonality of the hue versus lightness axes (Fig. 6A). Shepard plots revealed that the first three dimensions of cMDS space corresponded well to the patch distances found on the cortical surface (Fig. S6A). We fit lines along the lightness axis for each individual hue (including the achromatic lightness axis). We fit a plane to the line-centers of these lightness axes, defining the hue plane. We determined the angles between each lightness line to the normal vector of the hue plane: 0.75 ± 10.32 and 8.95 ± 11.65 degrees (mean ± SEM, n = 12) in the two monkeys, respectively. The lightness axes were very close to the normal vector, indicating that the hue and lightness dimensions are orthogonal in high-dimensional space.

A non-classical MDS analysis also revealed orthogonality between the hue and lightness dimensions of color representation on V1. Here, we embedded the response dissimilarity between cells—as a function of all color stimuli tested—into the first three MDS dimensions and found the relationship between hue and lightness to form a spherical surface (Bohon et al., 2016). Hues distributed themselves along the equator of the sphere, whereas lightness was distributed along the meridians, indicating orthogonality (Fig. 6B, see Materials and Methods, Shepard plot on Fig. S6B). Previous studies revealed similar results in area PIT (Bohon et al., 2016).

We conclude from all the above analyses that the V1 representations of hue and lightness are orthogonal to each other, similarly to the V1 representations of orientation and spatial frequency (Nauhaus et al., 2012).

3.6 The overall representation of perceptual color space in V1

We next determined whether the cortical representation of hue and lightness reflected the perceptual relationships of color vision. To do this, we computed the correlation between the cortical distances of hue and lightness patches versus perceptual DeltaEs in various color spaces. The correlation coefficients were significant (Fig. 6C). Further, the coefficients of near-uniform color spaces were significantly higher than DKL or CIExyY color spaces (Fig. 6D), indicating that V1 represents color perception much better than previously thought (Conway, 2014).

The dissimilarities-based MDS space created by our dissimilarity analyses of the hue, lightness, and achromatic lightness dimensions, also parallels the MDS space found previously in the PIT cortex (Bohon et al., 2016). This further suggests that the hue and lightness dimensions of color perception are already well represented in V1. We note that our results have a more apparent hue-lightness structure than the previous PIT results, perhaps due to our chosen stimulus set or to the increased cell numbers in our study.

In our dissimilarities-based MDS space analyses, we found that chroma did not change the position of points within the first three dimensions, indicating that chroma varies the response intensity, but not the position, within higher-dimensional space (Fig 3).

The comparison of the distance versus dissimilarity MDS analyses (Fig. 6A versus Fig. 6B, respectively) reveals that the distances between cortical patches recreates the barrel-like perceptual Munsell space, whereas the dissimilarity analyses revealed a spherical relationship. This suggests that Munsell color space are appropriate to the study of the cortical representation of color perception in V1.

3.7 Color responses of V1 cells are better explained by near uniform color spaces

We statistically determined that V1 cortical color space representations were better represented by Munsell than DKL color space by fitting each cell's response to color stimuli to each color space's characteristic variable, using multiple linear regression. This resulted in R^2 goodness-of-fit measures of DKL-based versus Munsel-based models, as well as additional fits to other color space models as well: CIExyY, CIELUV and CIELAB (Fig. 7A and Fig S7). All tested color spaces perform significantly better than DKL color space (one-tailed *t*-test, $p < 0.001$). This was especially robust for near uniform color spaces performs better than CIExyY color space, which follows from the correlations we found between cortical distances and neural signal similarities and DeltaE in various color spaces (Fig. 6C and 6D). When we performed these same linear regression analyses using only the equiluminant color plane, Munsell color space performed as well as DKL color space, and indeed was slightly, but significantly, superior to DKL (Fig. S7D).

We further examined the spatial distribution of those cells that are better explained by Munsell colors space or DKL color space (Fig.7B, see Materials and Methods). Whereas most cells are better explained by Munsell color space (84% and 92.7% in monkey A and B), we did find that when cells were better fit to DKL space, they were generally confined to cortical regions in which color or orientation tuned fields overlap on the maps (Fig.7.B-D), whereas Munsell-preferring cells were largely confined to color-tuned regions.

4 Discussion

The present study reveals a cortical representation of perceptual color space in V1. This representation not only includes the basic dimensions of color perception (hue, lightness, and chroma), but it also reflects the orthogonal relationships between hue and lightness perception. Our results provide the first evidence of a cortical map representing perceptual color space at processing stages earlier than the higher brain regions (Bohon et al., 2016; Conway, 2009; Liu et al., 2020), and thus our findings enhance our understanding of

the chromatic information processing abilities of V1 (Ng et al., 2007). The surprisingly perceptual-correspondence of V1 color representations may serve to provide the higher cortical areas with the initial organizing principles necessary to achieve even more advanced perceptual chromatic analyses, such as the lightness-invariant hue-selectivity found in PIT (Sanada et al., 2016). In addition, V1's contribution to color vision may help to explain how color is integrated with other types of visual information in the extrastriate cortex.

Local cortical signals from calcium dyes were previously used to study functional maps in NHP V1 (Nauhaus et al., 2012), though SNR was improved in the current study due to our lower background calcium signals. Local cortical GCaMP signals have been used to study ferret V1 with widefield epifluorescence, though with lower spatial resolution (Smith et al., 2015) than our mesoscale two-photon signals. The LoCa signals we employed here at micrometer resolution have high SNR, enhancing the quality of functional studies compared to previous methods. When used to map functional columns in V1, LoCa signals from a single imaging plane have higher utility than cellular imaging volumes (Figs. 2D–F, 3C and 4B) in two ways: (i) LoCa signal maps are more fine-grained than cellular maps; and (ii) LoCa signal imaging increases experimental efficacy more than 10 times when imaging stacks of more than 10 imaging planes. This high SNR also limits adaptation effects (Tailby et al., 2008) because stimuli do not need to be presented multiple times for each traditional imaging plane.

Chroma tuning has rarely been studied in V1, though a relationship between chroma and neuronal response magnitude was found previously in PIT (Conway, 2014). Using LoCa imaging, we found that V1 signal strength is also highly correlated to the perception of chroma (Fig. 3), in line with the results of a previous 14C-deoxy-d-glucose uptake study using color stimuli of different saturation levels (Tootell et al., 1988). We found a few neurons in our single-cell results that appeared to be selective for chroma, consistent with previous reports (Hanazawa et al., 2000). However, the proportion of cells exhibiting apparent chroma selectivity was very small and thus we cannot rule out a spurious correlation.

We discovered that V1 responses were more strongly correlated with color perceptual models of all three primary axes of color perception—hue, brightness, and chroma—than with the DKL color model. This suggests that the primary organizing principles of perceptual color space are established within V1, and that perceptual color spaces are best suited for color studies in V1.

Hue clusters have been reported previously within V1 using ISOI (Xiao et al., 2007). Our two-photon imaging data built on these results and revealed that hue representation in V1 forms pinwheel-like and linear-zone patterns. Hue clusters had a circular organization (Fig. 2) that followed from Munsell perceptual space color wheels (as well as other similar color spaces that have been used to describe human color perception). Complementing our high-resolution two-photon imaging, we employed evenly distributed colors from the color wheel of human perception, while holding chroma level stable. In previous studies, color stimuli were typically based on cone contrast, (Shapley, 2019) color spaces or the DKL system (Cottaris and De Valois, 1998), or they employed stimuli at the CRT's gamut

boundary (Garg et al., 2019; Xiao et al., 2007), which limited experimental control of the chroma dimension. Our results show that high saturation hues (such as the high chroma blues and reds that can be achieved by many CRTs) can produce saturated responses even in neurons that prefer other colors. Thus use of maximally saturated chroma levels leads to underestimation of the selectivity that a hue patch has with respect to other hues. It is therefore more conducive to use mid-level and carefully calibrated chroma levels to determine fine structures within hue preference and selectivity measures.

A previous study concluded that lightness level does not affect hue tuning in V1 cells (Thorell et al., 1984). Other research has instead found that hue and lightness are jointly encoded in V1 (Hass and Horwitz, 2013; Johnson et al., 2001; Lennie et al., 1990; Peng and Van Essen, 2005; Yoshioka et al., 1996). However, these prior studies used limited numbers of lightness levels and neuronal samples relative to our study. Our results may explain the previous discrepancy because we found that the maps for lightness encoding and hue encoding interact in orthogonal gradients on the cortex; thus, some hue-selective neurons will be unaffected by limited lightness levels whereas others will entangle hue with lightness, where the two gradients closely interact and cross. This coding strategy may facilitate the eventual appearance of hue-selective lightness invariant cells downstream of V1, such as those found in PIT (Conway et al., 2007).

In terms of the spatial relationship between hue and lightness patches, their relative cortical distances—together with chroma's effect on response strength—largely account for the three dimensions of perceptual color space enjoyed by old-world primates (Fig. 6A). This explanation potentially resolves the long-standing mystery of how a two-dimensional cortical map can represent three dimensions of color perception. Indeed, distance-based MDS analyses reveal a barrel-like color space in V1 that matches the shape of Munsell color space. Our dissimilarity based MDS results also support these conclusions, revealing a spherical shape to higher dimensional neuronal representations of color space.

Color and orientation maps are processed in parallel in V1 and share similar organizing principles in that they jointly encode multiple dimensions (Garg et al., 2019). Our discoveries suggest several new principles underlying the cortical organization of color and orientation in V1: (i) Color-selective fields are largely interdigitated with orientation-selective fields. Whereas orientation-selective fields were often aligned with the ocular dominance (OD) borders, color-selective fields tended to be aligned at the centers of OD columns. These findings were not reported in previous studies, perhaps because only two-photon imaging provides the high SNR and spatial resolution required to identify the specific hue-preferences at play on a sub-hypercolumn scale; (ii) The orthogonality of hue versus lightness representations in V1 is similar in nature to the orthogonal representations found previously between orientation and spatial frequency (Nauhaus et al., 2012); (iii) The contiguously spectral nature of perceptual color wheels was recapitulated by our hue pinwheels, just as the geometry of different orientations is systematically recapitulated in V1 according to the patterns found within orientation pinwheels. These organizing principles may contribute eventually to a universal theory of cortical information processing in V1 and beyond.

Although the advantages of two-photon imaging facilitated many of this study's discoveries, limitations remain. For example, the depth of recording with two-photon imaging remains constrained, challenging the experimenter's ability to precisely survey the functional structure throughout the cortical layers. The SNR with two-photon imaging is high but also remains limited, requiring many repeated presentations (~10) at each cortical location to obtain replicable functional results. This limitation prevents the use of the much larger stimulus sets that would permit finer grain analyses of the relationship between human perceptual color space and the maps in V1.

Supplementary Material

Refer to Web version on PubMed Central for supplementary material.

Acknowledgments

We thank Dr. Louis Tao in the early development of this study, Dr. Haidong Lu, Dr. Yu Cong and Dr. Wu Li in the comment of the manuscript.

Funding:

National Natural Science Foundation of China (grant no. 31730109，U1909205, to ST.)

National Basic Research Program of China (grant no. 2017YFA0105201, to ST.)

National Natural Science Foundation of China Outstanding Young Researcher Award (grant no. 30525016, to ST.)

Project 985 grant of Peking University, Beijing Municipal Commission of Science and Technology (grant no. Z18110000151, to ST.)

Fundamental Research Funds for the Central Universities (grant no. 2018NTST31, to ML.)

National Science Foundation (USA; Award 1734887 to SLM and SMC)

National Eye Institute (USA; Award R01- EY031971 to SMC and SLM)

References

Ankerst M, Breunig MM, Kriegel H-P, Sander J, 1999. OPTICS: Ordering Points to Identify the Clustering Structure. SIGMOD Rec 28, 49–60. 10.1145/304181.304187

Bohon KS, Hermann KL, Hansen T, Conway BR, 2016. Representation of Perceptual Color Space in Macaque Posterior Inferior Temporal Cortex (the V4 Complex). eNeuro 3. 10.1523/ENEURO.0039-16.2016

Chang L, Bao P, Tsao DY, 2017. The representation of colored objects in macaque color patches. Nat. Commun 8, 2064. 10.1038/s41467-017-01912-7 [PubMed: 29234028]

Chen T-W, Wardill TJ, Sun Y, Pulver SR, Renninger SL, Baohan A, Schreiter ER, Kerr RA, Orger MB, Jayaraman V, Looger LL, Svoboda K, Kim DS, 2013. Ultrasensitive fluorescent proteins for imaging neuronal activity. Nature 499, 295–300. 10.1038/nature12354 [PubMed: 23868258]

Conway BR, 2014. Color signals through dorsal and ventral visual pathways. Vis. Neurosci 31, 197–209. 10.1017/S0952523813000382 [PubMed: 24103417]

Conway BR, 2009. Color vision, cones, and color-coding in the cortex. Neuroscientist 15, 274–290. 10.1177/1073858408331369 [PubMed: 19436076]

Conway BR, Moeller S, Tsao DY, 2007. Specialized Color Modules in Macaque Extrastriate Cortex. Neuron 56, 560–573. 10.1016/j.neuron.2007.10.008 [PubMed: 17988638]

Conway BR, Tsao DY, 2009. Color-tuned neurons are spatially clustered according to color preference within alert macaque posterior inferior temporal cortex. Proc. Natl. Acad. Sci 106, 18034–18039. 10.1073/pnas.0810943106 [PubMed: 19805195]

Cottaris NP, De Valois RL, 1998. Temporal dynamics of chromatic tuning in macaque primary visual cortex. Nature 395, 896–900. 10.1038/27666 [PubMed: 9804422]

Dacey DM, 1996. Circuitry for color coding in the primate retina. Proc. Natl. Acad. Sci. U. S. A 93, 582–588. 10.1073/pnas.93.2.582 [PubMed: 8570599]

De Valois RL, Abramov I, Jacobs GH, 1966. Analysis of response patterns of LGN cells. J. Opt. Soc. Am 56, 966–977. 10.1364/JOSA.56.000966 [PubMed: 4959282]

De Valois RL, Cottaris NP, Elfar SD, Mahon LE, Wilson JA, 2000. Some transformations of color information from lateral geniculate nucleus to striate cortex. Proc Natl Acad Sci U S A 97, 4997–5002. 10.1073/pnas.97.9.4997 [PubMed: 10781111]

Derrington AM, Krauskopf J, Lennie P, 1984. Chromatic mechanisms in lateral geniculate nucleus of Macaque. J. Physiol 357, 241–65. 10.1113/jphysiol.1984.sp015499 [PubMed: 6512691]

Freiwald WA, 2020a. The neural mechanisms of face processing: cells, areas, networks, and models. Curr. Opin. Neurobiol 60, 184–191. 10.1016/j.conb.2019.12.007 [PubMed: 31958622]

Freiwald WA, 2020b. Social interaction networks in the primate brain. Curr. Opin. Neurobiol 65, 49–58. 10.1016/j.conb.2020.08.012 [PubMed: 33065333]

Friedman HS, Zhou H, von der Heydt R, 2003. The coding of uniform colour figures in monkey visual cortex. J. Physiol 548, 593–613. 10.1113/jphysiol.2002.033555 [PubMed: 12611925]

Garg AK, Li P, Rashid MS, Callaway EM, 2019. Color and orientation are jointly coded and spatially organized in primate primary visual cortex. Science (80-.) 364, 1275–1279. 10.1126/science.aaw5868

Gouras P, 1968. Identification of cone mechanisms in monkey ganglion cells. J. Physiol 199, 533–547. 10.1113/jphysiol.1968.sp008667 [PubMed: 4974745]

Graftieaux L, Michard M, Grosjean N, 2001. Combining PIV, POD and vortex identification algorithms for the study of unsteady turbulent swirling flows. Meas. Sci. Technol 12, 1422–1429. 10.1088/0957-0233/12/9/307

Hanazawa A, Komatsu H, Murakami I, 2000. Neural selectivity for hue and saturation of colour in the primary visual cortex of the monkey. Eur. J. Neurosci 12, 1753–1763. 10.1046/j.1460-9568.2000.00041.x [PubMed: 10792452]

Hasantash M, Lafer-Sousa R, Afraz A, Conway BR, 2019. Paradoxical impact of memory on color appearance of faces. Nat. Commun 10, 1–10. 10.1038/s41467-019-10073-8 [PubMed: 30602773]

Hass CA, Horwitz GD, 2013. V1 mechanisms underlying chromatic contrast detection. J. Neurophysiol 109, 2483–2494. 10.1152/jn.00671.2012 [PubMed: 23446689]

Hiramatsu C, Melin AD, Allen WL, Dubuc C, Higham JP, 2017. Experimental evidence that primate trichromacy is well suited for detecting primate social colour signals. Proc. R. Soc. B 284, 20162458. 10.1098/rspb.2016.2458

Horwitz GD, Hass CA, 2012. Nonlinear analysis of macaque V1 color tuning reveals cardinal directions for cortical color processing. Nat. Neurosci 15, 913–919. 10.1038/nn.3105 [PubMed: 22581184]

Indow T, Kanazawa K, 1960. Multidimensional mapping of Munsell colors varying in hue, chroma, and value. J. Exp. Psychol 59, 330–336. 10.1037/h0044796 [PubMed: 13852802]

Johnson EN, Hawken MJ, Shapley R, others, 2001. The spatial transformation of color in the primary visual cortex of the macaque monkey. Nat. Neurosci 4, 409–416. [PubMed: 11276232]

Ju N, Jiang R, Macknik SL, Martinez-Conde S, Tang S, 2018. Long-term all-optical interrogation of cortical neurons in awake-behaving nonhuman primates. PLOS Biol 16, e2005839. [PubMed: 30089111]

Ju N, Li Y, Liu F, Jiang H, Macknik SL, Martinez-Conde S, Tang S, 2020. Spatiotemporal functional organization of excitatory synaptic inputs onto macaque V1 neurons. Nat. Commun 11, 697. 10.1038/s41467-020-14501-y [PubMed: 32019929]

Komatsu H, Ideura Y, Kaji S, Yamane S, 1992. Color selectivity of neurons in the inferior temporal cortex of the awake macaque monkey. J. Neurosci 12, 408–424. 10.1523/JNEUROSCI.12-02-00408.1992 [PubMed: 1740688]

Kremkow J, Jin J, Wang Y, Alonso JM, 2016. Principles underlying sensory map topography in primary visual cortex. Nature 533, 52–57. 10.1038/nature17936 [PubMed: 27120164]

Landisman CE, Ts'o DY, 2002. Color processing in macaque striate cortex: Relationships to ocular dominance, cytochrome oxidase, and orientation. J. Neurophysiol 87, 3126–3137. [PubMed: 12037213]

Lee K-S, Huang X, Fitzpatrick D, 2016. Topology of ON and OFF inputs in visual cortex enables an invariant columnar architecture. Nature 533, 90–94. 10.1038/nature17941 [PubMed: 27120162]

Lennie P, Krauskopf J, Sclar G, 1990. Chromatic mechanisms in striate cortex of macaque. J. Neurosci 10, 649–69. [PubMed: 2303866]

Li M, Liu F, Jiang H, Lee TS, Tang S, 2017a. Long-Term Two-Photon Imaging in Awake Macaque Monkey. Neuron 93, 1049–1057.e3. 10.1016/j.neuron.2017.01.027 [PubMed: 28215557]

Li M, Liu F, Jiang H, Lee TS, Tang S, 2017b. Long-Term Two-Photon Imaging in Awake Macaque Monkey. Neuron 93, 1049–1057.e3. 10.1016/j.neuron.2017.01.027 [PubMed: 28215557]

Li M, Liu F, Juusola M, Tang S, 2014. Perceptual Color Map in Macaque Visual Area V4. J. Neurosci 34, 202–217. 10.1523/JNEUROSCI.4549-12.2014 [PubMed: 24381282]

Liu Y, Li M, Zhang X, Lu Y, Gong H, Yin J, Chen Z, Qian L, Yang Y, Andolina IM, Shipp S, Mcloughlin N, Tang S, Wang W, 2020. Hierarchical Representation for Chromatic Processing across Macaque V1, V2, and V4. Neuron 108, 538–550.e5. 10.1016/j.neuron.2020.07.037 [PubMed: 32853551]

Livingstone M, Hubel D, 1988. Segregation of form, color, movement, and depth: anatomy, physiology, and perception. Science (80-.) 240, 740–749. 10.1126/science.3283936

Livingstone MS, Hubel DH, 1984. Anatomy and physiology of a color system in the primate visual cortex. J. Neurosci 4, 309–56. 10.1523/jneurosci.04-01-00309.1984 [PubMed: 6198495]

Livingstone MS, Hubel DH, 1983. Specificity of cortico-cortical connections in monkey visual system. Nature 304, 531–534. 10.1038/304531a0 [PubMed: 6308468]

Munsell AH, 1919. A color notation Munsell color company.

Nauhaus I, Nielsen KJ, Disney AA, Callaway EM, 2012. Orthogonal micro-organization of orientation and spatial frequency in primate primary visual cortex. Nat. Neurosci 15, 1683–90. 10.1038/nn.3255 [PubMed: 23143516]

Ng J, Bharath AA, Zhaoping L, 2007. A survey of architecture and function of the primary visual cortex (V1). EURASIP J. Adv. Signal Process 2007. 10.1155/2007/97961

Osorio D, Vorobyev M, 1996. Colour Vision as an Adaptation to Frugivory in Primates. Proc. R. Soc. B Biol. Sci 263, 593–599. 10.1098/rspb.1996.0089

Peng X, Van Essen DC, 2005. Peaked encoding of relative luminance in macaque areas V1 and V2. J. Neurophysiol 93, 1620–32. 10.1152/jn.00793.2004 [PubMed: 15525807]

Sanada TM, Namima T, Komatsu H, 2016. Comparison of the color selectivity of macaque V4 neurons in different color spaces. J. Neurophysiol 116, 2163–2172. 10.1152/jn.00108.2016 [PubMed: 27535368]

Shapley R, 2019. Physiology of Color Vision in Primates, in: Oxford Research Encyclopedia of Neuroscience Oxford University Press, pp. 1–35. 10.1093/acrefore/9780190264086.013.74

Shapley R, Hawken MJ, 2011. Color in the Cortex: Single- and double-opponent cells. Vision Res 51, 701–717. 10.1016/j.visres.2011.02.012 [PubMed: 21333672]

Shepherd SV, Freiwald WA, 2018. Functional Networks for Social Communication in the Macaque Monkey. Neuron 99, 413–420.e3. 10.1016/j.neuron.2018.06.027 [PubMed: 30017395]

Sincich LC, Horton JC, 2005. THE CIRCUITRY OF V1 AND V2: Integration of Color, Form, and Motion. Annu. Rev. Neurosci 28, 303–326. 10.1146/annurev.neuro.28.061604.135731 [PubMed: 16022598]

Sliwa J, Freiwald WA, 2017. A dedicated network for social interaction processing in the primate brain. Science (80-.) 356, 745–749. 10.1126/science.aam6383

Smith GB, Whitney DE, Fitzpatrick D, 2015. Modular Representation of Luminance Polarity in the Superficial Layers of Primary Visual Cortex. Neuron 88, 805–818. 10.1016/j.neuron.2015.10.019 [PubMed: 26590348]

Stockman A, Brainard DH, 2010. COLOR VISION MECHANISMS, in: Bass M (Ed.), Handbook of Optics McGraw-Hill.

Stockman A, Sharpe LT, 2000. The spectral sensitivities of the middle- and long-wavelength-sensitive cones derived from measurements in observers of known genotype. Vision Res 40, 1711–1737. 10.1016/S0042-6989(00)00021-3 [PubMed: 10814758]

Tailby C, Solomon SG, Dhruv NT, Lennie P, 2008. Habituation reveals fundamental chromatic mechanisms in striate cortex of macaque. J. Neurosci 28, 1131–1139. 10.1523/JNEUROSCI.4682-07.2008 [PubMed: 18234891]

Thorell LG, de Valois RL, Albrecht DG, 1984. Spatial mapping of monkey VI cells with pure color and luminance stimuli. Vision Res 24, 751–769. 10.1016/0042-6989(84)90216-5 [PubMed: 6464367]

Tootell R, Silverman M, Hamilton S, De Valois R, Switkes E, 1988. Functional anatomy of macaque striate cortex. III. Color. J. Neurosci 8, 1569–1593. 10.1523/JNEUROSCI.08-05-01569.1988 [PubMed: 3367211]

Ts'o D, Gilbert C, 1988. The organization of chromatic and spatial interactions in the primate striate cortex. J. Neurosci 8, 1712–1727. 10.1523/jneurosci.08-05-01712.1988 [PubMed: 3367218]

Wachtler T, Sejnowski TJ, Albright TD, 2003. Representation of color stimuli in awake macaque primary visual cortex. Neuron 37, 681–691. 10.1016/S0896-6273(03)00035-7 [PubMed: 12597864]

Williams EJ, 1959. The Comparison of Regression Variables. J. R. Stat. Soc. Ser. B 21, 396–399. 10.1111/j.2517-6161.1959.tb00346.x

Xiao Y, Casti A, Xiao J, Kaplan E, 2007. Hue maps in primate striate cortex. Neuroimage 35, 771–786. 10.1016/j.neuroimage.2006.11.059 [PubMed: 17276087]

Xiao Y, Wang Y, Felleman DJ, 2003. A spatially organized representation of colour in macaque cortical area V2. Nature 421, 535–539. 10.1038/nature01372 [PubMed: 12556893]

Yoshioka T, Dow BM, Vautin RG, 1996. Neuronal mechanisms of color categorization in areas V1, V2 and V4 of macaque monkey visual cortex. Behav. Brain Res 76, 51–70. 10.1016/0166-4328(95)00183-2 [PubMed: 8734043]

Zack GW, Rogers WE, Latt SA, 1977. Automatic measurement of sister chromatid exchange frequency. J. Histochem. Cytochem 25, 741–753. 10.1177/25.7.70454 [PubMed: 70454]

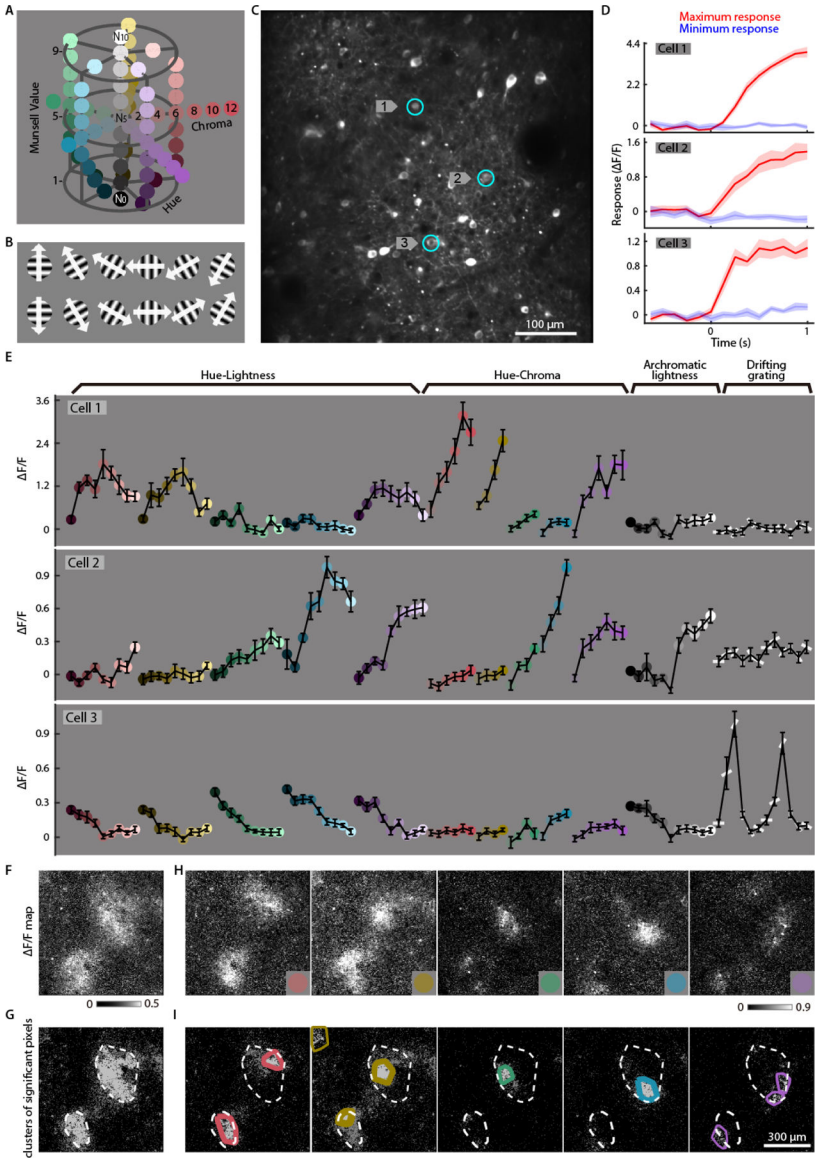

Fig. 1. Stimulus set, single-cell calcium signal, and local cortical calcium (LoCa) signals.

(**A**) The color stimulus set contains 11 achromatic lightness colors (Munsell color N_0 to N_{10}), 4–7 chroma levels (Chroma = 2 to 14) with a Munsell Value (lightness) of 5 for each hue, and 9 lightness levels for each hue (Munsell Chroma = 6). Color stimuli were presented as round static disks on CRT. (**B**) Twelve achromatic drifting gratings were also included in the stimuli set. The arrows indicate the directions of the drifting gratings. (**C**) An exemplar two-photon image (average of a time series) from a 25x objective lens. (**D**) Time course of response (mean ± STE from N = 10 trials) from the exemplar cells shown in (C) for the most preferred stimulus (red line) versus the least preferred stimulus (blue line). (**E**) Mean responses (± STE, N = 10 trials for each stimulus) as a function of stimuli from the cells indicated in (C). Each data point corresponds to a stimulus from (A) or (B). (**F**) Averaged LoCa signals (*ΔF/F* map) evoked by five hues (Munsell 5R, 5Y, 5G, 5B, or 5P, Value = 5, Chroma = 6). (**G**) Significant pixels in (F) (one-tailed *t*-test for paired samples,

$p < 0.01$) are shown in gray. Highlighted pixels in bright gray are patches clustered by the OPTICS algorithm. Contoured convex-hulls indicate the patches in the following analysis. (**H-I**) LoCa signals are highly effective in revealing cortical locations activated by different hues. Dashed contours are copied from (G). The thickness of the colored contours indicates the relative signal strength of pixels within that contour.

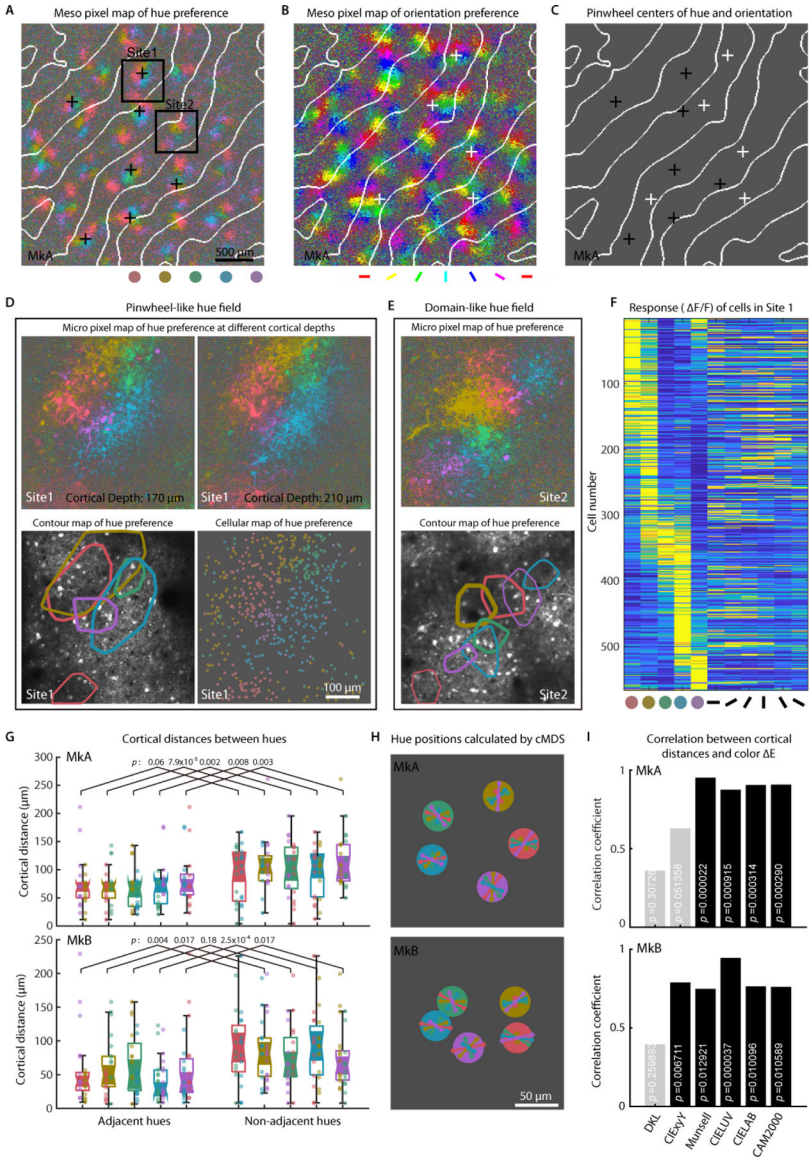

Fig. 2. Circular representation of hues in V1.

(**A**) Mesoscale pixel map of hue preference. Each pixel is rendered by the hue that evoked the maximum response (4x objective, N= 50 trials for each stimulus). White lines indicate the border of ocular dominance (OD) columns. Pinwheel centers are marked by black crosses. The eccentricity of this cortical location was around 4.7°. (**B**) Mesoscale pixel orientation preference map. Pseudo colors denote orientation. Pinwheel centers are marked by white crosses. (**C**) Pinwheel centers for hue versus orientation are presented on a single map. (**D**) Site 1 in (A) was magnified with a 25x objective lens across 7 cortical depths (80 – 250 μm). Pinwheel-like patterns were verified by three different analysis modalities to determine that analysis artifacts do not explain the results: micro pixel maps, contour maps, and cellular maps. The thickness of the colored contours indicates the relative signal strength of the pixels within the contour. (**E**) Exemplar linear-zone-like color fields (Site 2 from (A)). (**F**) Response heat maps of hues versus orientations from each cell in (D), sorted

by hue, reveal no systematic relationship between color tuning and orientation tuning. (**G**) Pairwise measurements between patches of non-adjacent hues reveal larger cortical distances than between spectrally adjacent hues (one-tailed Wilcoxon rank-sum test, $p < 0.05$ in 8 of 10 pairs). The notches indicate median ± 1.57 * IQR / sqrt(n), n = 24 – 28. (**H**) Median cortical distances between any pair of hues embedded within 2-dimensional cMDS space. Stress = 0.06 and 0.13 for monkeys A and B, respectively. The lines on the circles are error bars indicating the distances between patches of two hues (± 1.57 * IQR / sqrt(n)). Data derive from a 2 mm x 2 mm cortical area shown in Fig. S2D. (**I**) Cortical distances between hues are highly correlated with ΔE in near-uniform Munsell, as well as CIELUV, CIELAB, and CAM2000 perceptual color space in both monkeys. Correlation coefficient bars with $p < 0.05$ are in black, otherwise gray.

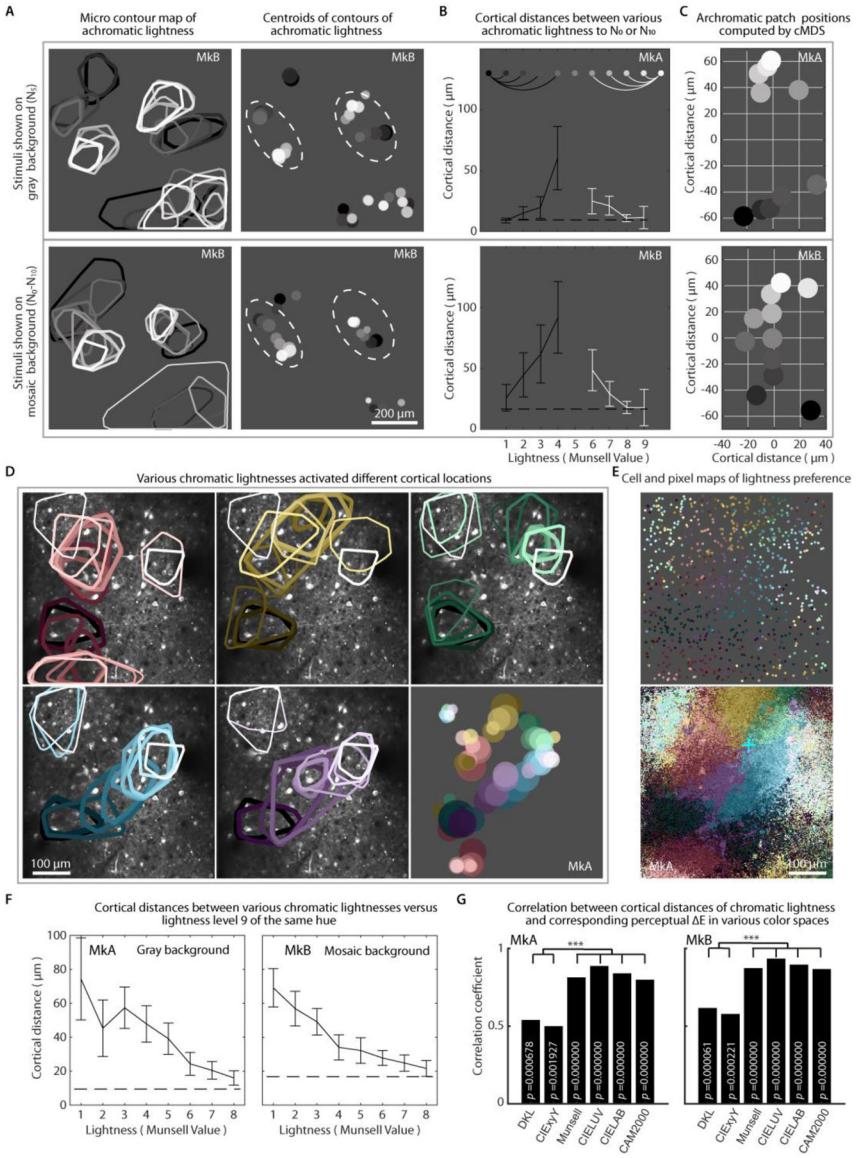

Fig. 3. Perceptual lightness is represented in a gradient across cortical locations.

(**A**) Patches of achromatic lightness form black and white groups when the stimuli are shown against a homogenous gray background; at the same cortical location, when stimuli were shown against a mosaic background, the patches of different achromatic lightness formed linear-zone-like clusters. Centroids of contours on the left panels are shown as disks on the right panels. The disk size indicates the relative signal strength of each patch. (**B**) The median cortical distances between achromatic patches ranging in lightness between N_0 - N_{10} exhibit similar distributions under either gray or mosaic backgrounds. Data from Mk A and B, respectively, n = 15 – 25 clusters. (**C**) 2D cMDS analysis reveals significant differences between the two background conditions employed. Stresses at dimension 2 are 0.011 and 0.005, respectively. Data come from the cortical area in Fig. S2D. (**D**) Contours indicating different lightnesses of varied hues exhibit systematic displacement on the cortex. Contour centroids are shown as disks on the bottom right panel (disk size indicates the

relative signal strength of each contour). The thickness of the colored contours indicates the relative signal strength of pixels within the contour. (**E**) Traditional cellular response maps and pixel maps are consistent with the contour map in (D), indicating that the results are not an analysis artifact. The pinwheel center is indicated by a cyan cross. Cells or pixels are labeled by their most preferred stimulus (maximum response). (**F**) The average lightness contour distance from lightness Value 9 reveals that lightness maps follow a graded pattern (distances between the five different hues are averaged, and do not include the achromatic patches). Data are shown as median ± 1.57 * IQR / sqrt(n), n= 53–74 for monkey A, 79 – 94 for monkey B. The dashed line represents the median displacement of patches activated by the same colors (five hues, Munsell Chroma = 6, Value = 5) of different trials. (**G**) The cortical distances between patches of different lightnesses of various hues are positively correlated to the perceptual DeltaE between colors described in various color spaces. The correlation coefficient is significantly higher in the near-uniform perceptual color spaces than in DKL or CIExyY color spaces (n = 36). Correlation coefficients were compared using a one-tailed Williams' *t*-test for overlapping dependent data, with Bonferroni correction. Significance level, *** = 0.001.

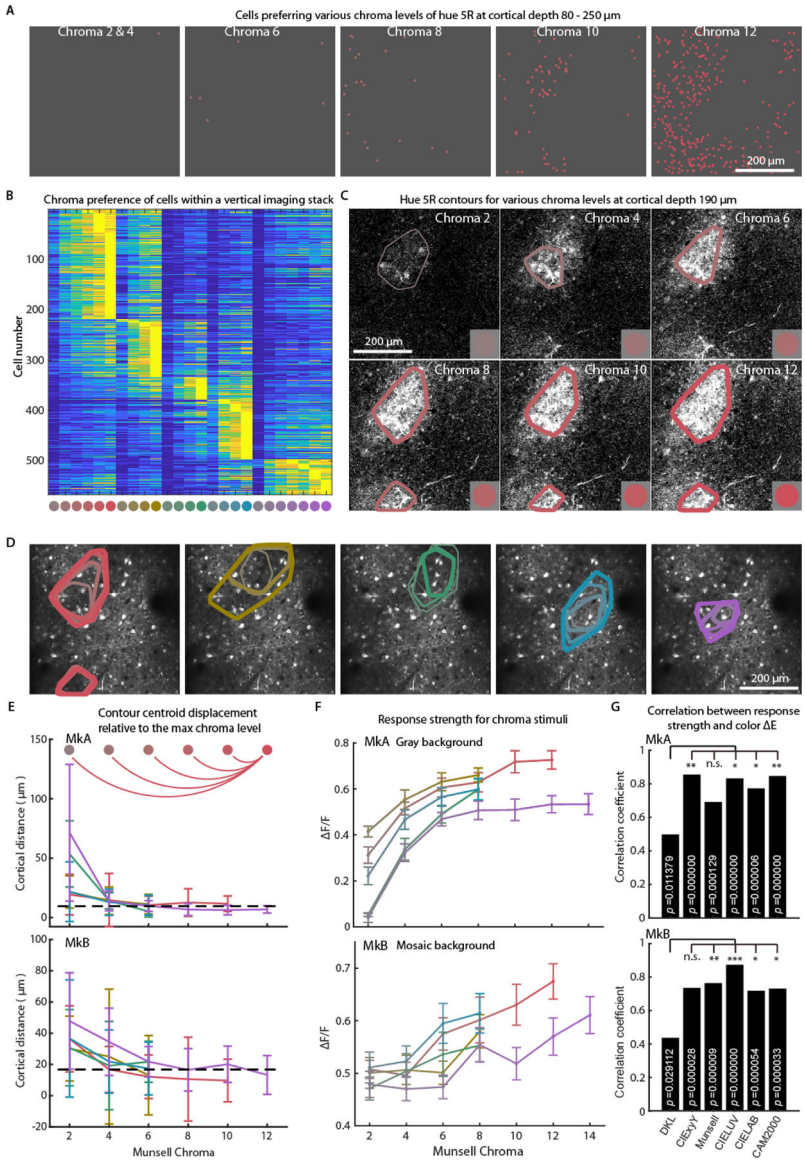

Fig. 4. Chroma is represented in V1 by the strength of neural response.

(**A**) Cells that have the maximum response at various chroma levels of Munsell hue 5R are shown on each map. The same cortical location with Fig. 2D. (**B**) Response heat maps from cells at the same location of Fig. 2D as a function of chroma levels for each of the five tested hues. Most of the cells have a maximum response for the highest chroma levels. (**C**) Micro pixel map and contour map for various chroma levels of Munsell hue 5R show activation of the same cortical locations with different strengths (same cortical area as (A)). (**D**) Contour map for five hues at different chroma levels (same cortical area as (A)). The thickness of the colored contours indicates the relative signal strength of pixels within each contour. (**E**) Contour centroids distances between patches activated by various chroma levels to those by the maximum chroma level. At chroma levels > 6, displacements reach baseline (dashed line). The dashed line represents the median displacement of patches activated by the same colors (five hues, Munsell Chroma = 6, Value = 5) of different trials. (**F**) Response

strength as a function of chroma level (mean ± SEM, n = 3 – 29 patches in monkey A, 22 – 39 patches in monkey B). (**G**) Neural response strength was positively correlated with the perceptual DeltaE described by various color spaces, especially in near-uniform perceptual color space (n = 25). Correlation coefficients were compared by a one-tailed Williams test for overlapping dependent data, with Bonferroni correction. Significance level: * = 0.05; ** = 0.01; *** = 0.001.

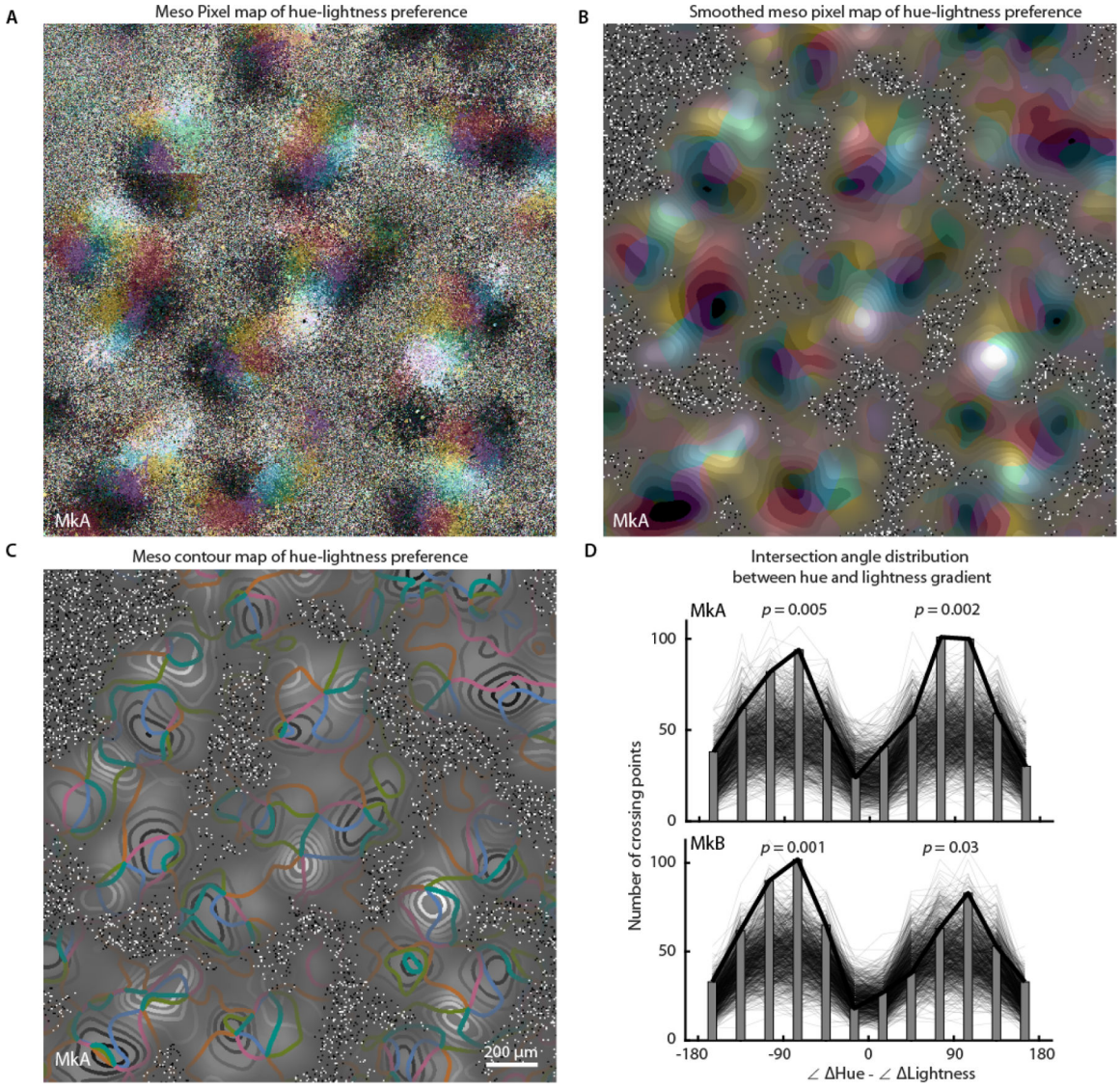

Fig. 5. Cortical Representations for Hue and Lightness are Orthogonal to Each Other.

(**A**) Pixel map for hue-lightness preference of a 2 mm x 2 mm area. (**B**) Smoothed pixel map for hue-lightness preference (Gaussian low pass filter, σ = 35 μm). (**C**) Contour map of (B) showing that hue and lightness gradients cross each other orthogonally. Colored curves represent hue contours, and achromatic curves represent lightness contours. (**D**) Histograms showing the distribution of the intersection angle between hue and lightness map gradients at each crossing point in (C) (regions where SNRs < 3 are not included). Thick lines describe the envelope of the histogram. Thin pale lines describe the envelope of histograms produced by 1000 times random permutation of color stimuli labels. All the peaks are significant (p < 0.05).

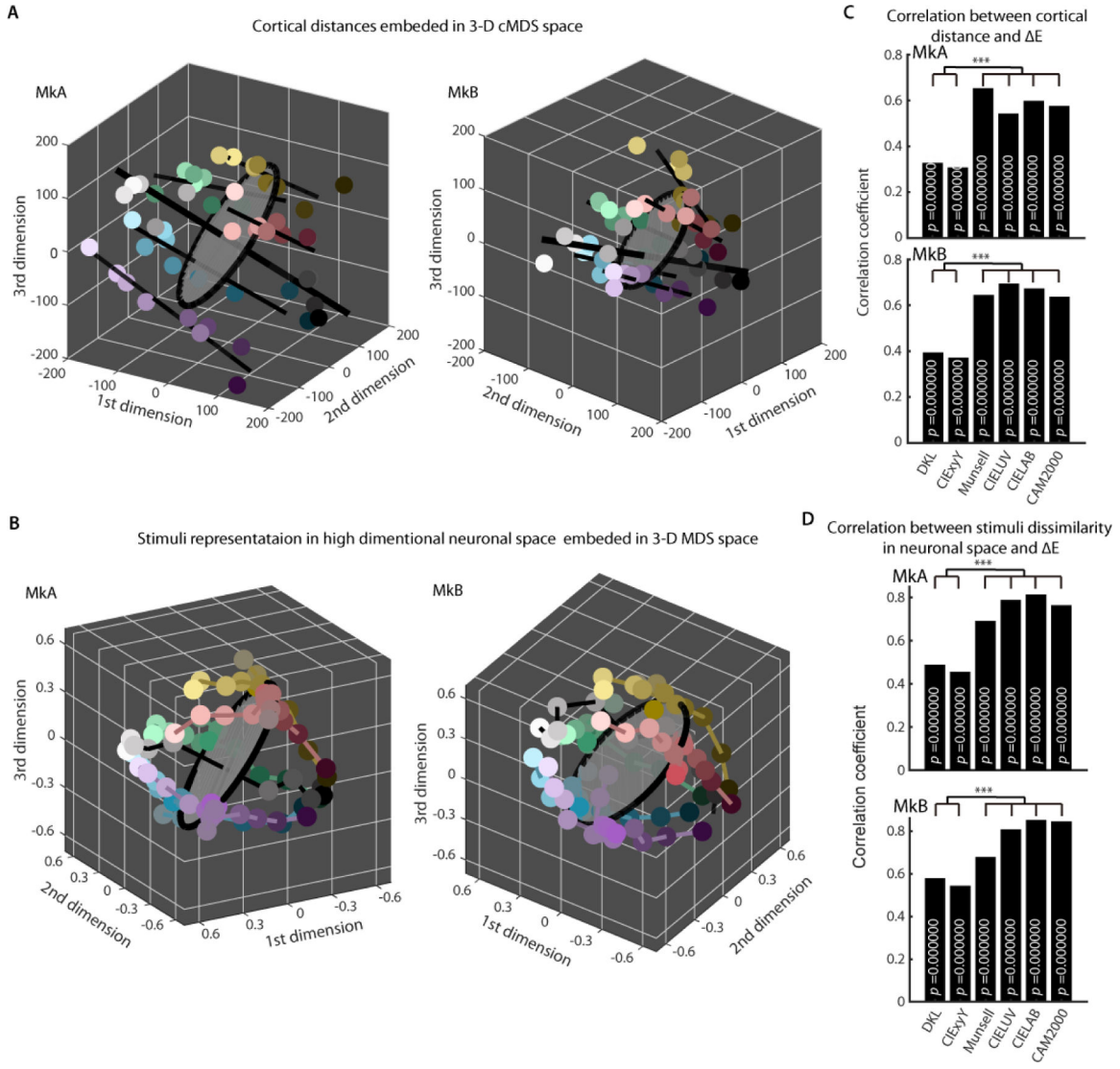

Fig. 6. The reconstructed color space by MDS using the cortical distances or neural response.

(**A**) Classical multiple dimensional scaling (cMDS) analysis of median distances between patches for each combination of hue and lightness, including achromatic lightness. The cMDS stress of the third dimension is 0.03 and 0.02 for the two monkeys, respectively. See Fig. S6A for the Shepard plot of this reconstruction. (**B**) Dissimilarities between the color stimuli in the high dimensional neuronal space were embedded in non-classical MDS space. 2127 and 1412 cells from monkeys A and B were used. Stress = 0.01 for both monkeys at the third dimension. See Fig. S6B for the Shepard plot of this reconstruction. (**C**) Correlations between the cortical distances of hue-lightness patches and DeltaE in various color spaces. (**D**) Correlations between stimulus dissimilarities in the high dimensional neuronal space and DeltaE in various color spaces. Correlation coefficients were compared by a one-tailed Williams test for overlapping dependent data, with Bonferroni correction. Significance level: *** = 0.001.

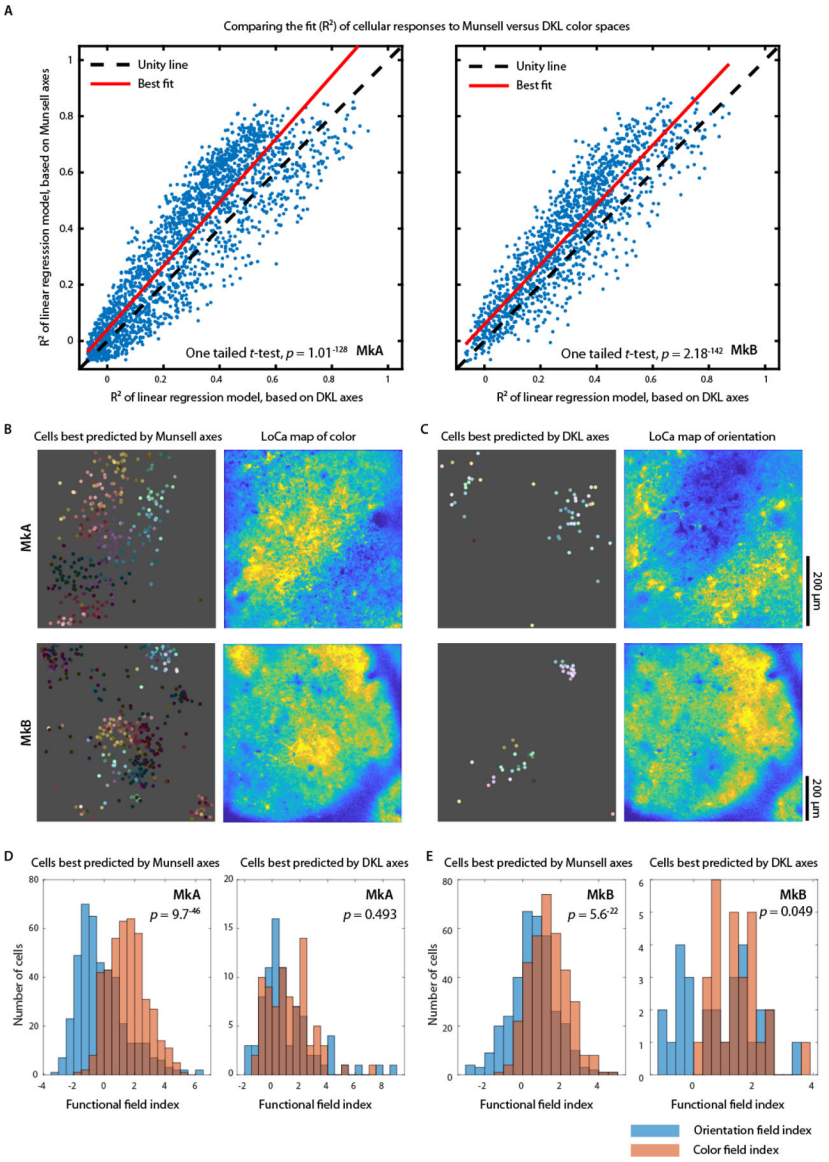

Fig. 7. V1 color cells are better explained by near uniform color space.

(**A**) Responses of each cell fit by multiple linear regression, using coordinates from Munsell versus DKL color spaces. R^2 of the fits indicate that Munsell based models describe the data significantly better than DKL based models in both monkeys (one-tailed *t*-test, $p < 0.001$). See Fig. S7 for further comparations of DKL based model versus other color spaces. (**B-C**) Exemplar recording sites showing distribution of cells that are best explained by Munsell versus DKL axes. LoCa maps of color versus orientation responses (right column) for comparison to the cellular data (left column). (**D-E**) Functional field indices showing cellular fits to color versus orientation fields as a function of using Munsell versus DKL color spaces. Cells were sampled from 9 imaging planes in monkey A and B respectively. The *p*-values of *t*-test are shown on the top right corner.

Table 1.

Coordinates of chroma color stimuli (in CIE_1931 xyY).

	5R		5Y		5G		5B		5P	
		xyY		xyY		xyY		xyY		xyY
V5	C2	0.3391 0.3192 20.89	C2	0.3505 0.3628 20.53	C2	0.2972 0.3393 20.51	C2	0.2793 0.3039 20.55	C2	0.3042 0.2925 20.41
V5	C4	0.3739 0.3221 20.69	C4	0.3922 0.4061 20.68	C4	0.2839 0.3625 20.56	C4	0.2496 0.2878 20.54	C4	0.2989 0.2696 20.47
V5	C6	0.4080 0.3234 20.91	C6	0.4294 0.443 20.54	C6	0.2684 0.3844 20.43	C6	0.2211 0.2696 20.44	C6	0.294 0.2496 20.59
V5	C8	0.4417 0.3244 20.8	C8	0.4577 0.4683 20.75	C8	0.251 0.4104 20.75	C8	0.1956 0.2511 20.71	C8	0.2891 0.2303 20.67
V5	C10	0.4747 0.3225 20.82							C10	0.2841 0.2133 20.83
V5	C12	0.5073 0.3195 20.89							C12	0.2806 0.1966 20.59
V5									C14	0.2781 0.1847 20.41

Table 2.

Coordinates of hue-lightness color stimuli (in CIE_1931 xyY).

	5R		5Y		5G		5B		5P		N
		xyY		xyY		xyY		xyY		xyY	xyY
V0		–		–		–		–		–	0.283 0.322 0.332
V1	**C3.7**	0.435 0.277 1.250	**C1.8**	0.408 0.415 1.290	**C3**	0.262 0.387 1.300	**C2.5**	0.212 0.253 1.278	**C5**	0.284 0.177 1.289	0.310 0.315 1.510
V2	**C6**	0.465 0.295 3.328	**C3.5**	0.435 0.440 3.190	**C5**	0.248 0.405 3.290	**C4**	0.205 0.252 3.300	**C6**	0.284 0.200 3.250	0.309 0.317 3.610
V3	**C6**	0.459 0.316 7.005	**C5**	0.443 0.451 6.840	**C6**	0.248 0.409 6.930	**C5**	0.201 0.252 6.830	**C6**	0.286 0.213 6.875	0.310 0.317 7.170
V4	**C6**	0.429 0.322 12.69	**C6**	0.446 0.454 12.71	**C6**	0.258 0.399 12.60	**C6**	0.207 0.258 12.70	**C6**	0.290 0.235 12.78	0.311 0.315 12.38
V5	**C6**	0.409 0.323 21.10	**C6**	0.429 0.444 21.11	**C6**	0.268 0.385 20.90	**C6**	0.221 0.270 21.10	**C6**	0.294 0.250 20.59	0.310 0.316 20.90
V6	**C6**	0.394 0.323 32.00	**C6**	0.415 0.431 31.60	**C6**	0.273 0.378 31.90	**C6**	0.232 0.279 31.90	**C6**	0.296 0.259 31.25	0.310 0.316 31.53
V7	**C6**	0.381 0.326 45.37	**C6**	0.403 0.421 45.90	**C6**	0.280 0.372 45.70	**C6**	0.240 0.285 46.01	**C6**	0.297 0.267 45.01	0.310 0.316 45.40
V8	**C6**	0.374 0.325 62.98	**C6**	0.392 0.413 62.30	**C6**	0.282 0.370 62.20	**C6**	0.245 0.289 62.50	**C6**	0.297 0.270 61.6	0.311 0.316 62.61
V9	**C3.5**	0.343 0.321 81.10	**C6**	0.385 0.407 82.30	**C6**	0.283 0.369 82.05	**C4**	0.267 0.300 82.23	**C4**	0.300 0.287 82.76	0.311 0.316 83.60
V10		–		–		–		–		–	0.310 0.317 106.8